Adv Polym Sci (2017) 276: 45–92
DOI: 10.1007/12_2016_350

Published online: 24 September 2016

Molecular View of Properties of Random Copolymers of Isotactic Polypropylene

Finizia Auriemma, Claudio De Rosa, Rocco Di Girolamo, Anna Malafronte, Miriam Scoti, and Claudia Cioce

Abstract The yield behavior during uniaxial drawing of isotactic random copolymers of propene with ethylene (iPPEt), 1-butene (iPPBu), 1-pentene (iPPPe), 1-hexene (iPPHe), and 1-octadecene (iPPOc) is analyzed within the framework of our current understanding of deformation properties of semicrystalline polymers, that is, the intrinsic stability of lamellar crystals and related polymorphism phenomena, along with the ability of entangled amorphous chains to transmit stress. The samples selected for analysis were synthesized using single-site metalorganic catalysts, are highly stereoregular, and contain small amounts of regiodefects caused by secondary 2,1 erythro units. Moreover, the interchain and intrachain distribution of comonomeric units is uniform. In the case of iPPEt copolymers, samples containing ≈3.5 mol% stereodefects were also studied. The yield behavior of these samples depends on the kind and concentration of defects, and is directly related to the level of inclusion in and exclusion from crystals of the comonomeric units. Apart from iPPBu copolymer samples with high butene content, the yield stress of all samples increases with the thickness of lamellar crystals according to a common trend, regardless of comonomer. In the case of iPPBu copolymers containing a high concentration of butene units, the yield stress decreases with increasing lamellar thickness. The increase in yield stress with lamellar thickness is rationalized in terms of the micromechanical model of crystallographic slips, based on thermal activation of screw dislocations. The parameters of the model describing the yield behavior are the critical free energy required to form a screw dislocation and the shear modulus associated with the slip planes of the dislocations. These were set as identical to those deduced for isotactic polypropylene homopolymer samples (iPP) crystallized under different conditions. Study of the yield behavior of

F. Auriemma (✉), C. De Rosa, R. Di Girolamo, A. Malafronte, M. Scoti, and C. Cioce
Dipartimento di Science Chimiche, Complesso Monte Sant' Angelo, via Cintia, 80126 Naples, Italy
e-mail: finizia.auiemma@unina.it

these copolymers extends the use of the dislocation model to a set of samples crystallized under similar conditions but characterized by differences in comonomeric unit, degree of crystallinity, lamellar thickness, polymorphism, and intrinsic flexibility of the chain backbone. The results indicate that for a homogeneous class of propene-based copolymers, namely crystallized in the α-form of iPP under similar conditions, lamellar thickness controls the level of plastic resistance provided that the concentration of structural irregularities in the crystals is not too high. iPPBu copolymers with high comonomer concentration do not obey this rule because of the high level of inclusion of comonomers in the crystals, which induces an increase in lamellar thickness but also a decrease in crystal stability.

Keywords Random copolymers • Yield behavior • Crystallographic slip process • Dislocation model • Polymorphism

Contents

1 Introduction

The uniaxial deformation of semicrystalline polymers having spherulitic or lamellar morphology transforms an initially isotropic material into oriented fibers. In semicrystalline polymers, the complex interwoven structure of amorphous and crystalline phases that are tightly intermingled [1] entails that the deformation process is complex [2, 3, 4, 5–9]. Deformation involves movement of atoms or groups of atoms, both in the crystalline and amorphous phase, in a cascade of events over different length scales. These range from the length scale of monomeric units, unit cells, and coils to the thickness of lamellar crystals, assembly of lamellae in stacks separated by amorphous phase, and spherulites [5, 7, 10–19]. The movements follow a common scheme during uniaxial stretching and involve both elastic (reversible) deformation and plastic (permanent) deformation as a result of viscous flow activated by the stress field [3, 5–7, 20, 21].

At low strains, the stress increases linearly and the polymer sample responds to the applied strain elastically, obeying Hooke's law [22]. The main mechanisms behind the Hooke regime of deformation occurring at the subnanometric length scale are the deformation of covalent bonds and valence angles, librational motion of internal rotation angles, and reversible deformation of unit cell axes [22, 25]. By

releasing the tension, the sample recovers its initial shape and dimensions. The proportionality constant between stress and strain is the Young's modulus, which depends mainly on the intrinsic flexibility of the chains and the volume fraction of the crystalline phase [22–24].

With further increase in strain, the stress within the polymer increases to reach the yield point. The high mobility achieved at the yield point initiates plastic (irreversible) deformation in the material, at a rate equal to the applied strain rate. After yielding, strain softening takes place, leading to strain localization and subsequent necking. From now on, plastic deformation dominates until break [5, 7, 26, 27].

The molecular mechanisms involved at yield and during plastic deformation up to the break point depend on the deformation rate, temperature, and crystallization conditions of the sample [5, 7, 27, 28]. Possible mechanisms associated with yielding behavior and plastic deformation of a polymer are partial melting and recrystallization [29, 30], thermal activation of screw dislocations with the Burgers vector parallel to the chain axis [6, 8, 14–19, 25, 31, 32], cavitation, and micronecking [3, 20, 21].

The concept that yielding and successive plastic deformation are the result of strain-induced melting of crystals followed by recrystallization into new crystals in adiabatic conditions (mechanical melting) was suggested by Yoon and Flory [29] on the basis of speculative considerations and not on experiments. According to this concept, the melting of initially unoriented crystals followed by recrystallization of the molten material into new crystals with a predominant chain orientation induced by strain is the thermodynamic driving force for plastic deformation, because it would allow reduction of the local stress level during drawing. Although this mechanism can explain the decrease in thickness and lateral dimensions of lamellar crystals during drawing, and the high degree of orientation achieved in a fiber, it does not account for the yielding process. Indeed, only after yielding does the stress-induced melting–recrystallization mechanism play some role in the plastic flow of a polymer [5–7]. The new crystals may either correspond to the same polymorph initially present in the sample or to a completely different polymorph [33–44]. It has been shown that occurrence of stress-induced polymorphic transitions during stretching produces a neat increase in ductility, because this provides a mechanism for conversion of mechanical energy into latent heat of fusion, which induces local melting of the crystals followed by recrystallization into a new phase [40–43].

By contrast, the crystallographic model based on thermal activation of screw dislocations is the most general and important micromechanical model of plastic deformation in polymers [23, 24, 31, 32, 35–37]. The mechanism of thermal activation of screw dislocations becomes effective from the yield point through occurrence of crystal slip processes, assisted by interlamellar slip in the amorphous layers. Moreover, for some polymers, additional twinning modes or stress-induced polymorphic transformations can also occur at high deformations [45–52]. Stress-induced phase transition, in turn, may occur not only through mechanical melting followed by recrystallization [29, 40, 41, 43, 44, 53], but can also be first-order as in martensitic (displacive) processes [35–45, 54–59]. The crystallographic

approach correctly predicts the dependence of the yield stress on the stem length of lamellae, temperature, and strain-rate [16, 60–67].

More precisely, the crystallographic approach to plastic deformation of semicrystalline polymers originates from basic ideas borrowed from the classical theory of crystal plasticity, that is, that the yield stress is governed by the energy required to nucleate a dislocation within a lamellar crystal [68–72]. Bowden and Young [25] adopted this idea and demonstrated that the picture based on classical concepts of nucleation of dislocations and their glide along the crystal lattice agrees well with the behavior of semicrystalline polymers [6, 8, 12–19, 25, 31, 32, 73–76].

According to this approach, the plastic deformation of polymer crystals is, in essence, of crystallographic origin and takes place without destroying the crystalline order. It occurs by crystallographic slips in the planes of closest packing (slip planes), generally corresponding to large interplanar distances, in directions coinciding with the direction of the closest packing located in the slip plane [25]. The slip mechanism is produced by the glide of a linear defect, namely a screw dislocation, along the slip plane. It can therefore accommodate plastic strains much more easily than other mechanisms such as twinning or martensitic transitions. The slip begins when the shear stress in the slip direction τ reaches a value higher than a threshold level that is critical for the given slip system. Such a stress level τ_0 corresponds to the critical resolved shear stress [5–7, 14–19, 25]. Thus, yielding starts when the critical resolved shear stress is reached in any family of lattice planes with low τ_0.

For polymer crystals, the slip systems need to operate in planes parallel to the chain axes. The most typical modes are chain slip involving a glide parallel to chain axes and transverse slip involving a glide perpendicular to chain axes (Fig. 1A, B). Additional constraints to the crystallographic deformation process are imposed by chain folds [5]. Chain folds should not be destroyed during deformation. Therefore, slip processes parallel to planes containing chain folds are generally preferred.

The slip process during deformation may occur in two different ways, producing either fine slips (Fig. 1D) or coarse slips (Fig. 1E) [7, 14–19, 49–52, 77–79]. Fine slips consist of displacements by one or two lattice vectors on every other lattice plane of a crystal [77–79]. With increased slip processes, the global effect results in a progressive increase in chain tilting with respect to the lamellar normal and a decrease in lamellar thickness (Fig. 1D). Coarse slips consist of significant shear displacements of crystal blocks on well-separated crystal planes. In general, coarse slips take place in lamellae containing a high concentration of defects or having a block fine-structure and in the late stages of deformation, when the crystals are already thinned as a result of advanced fine slip processes [77–79]. Eventually, at this stage of deformation, lamellae become so weak that they undergo slip instabilities, that is, complete fragmentation, orientation, destruction [32], and recrystallization in oriented crystals of fibrillar morphology.

The third micromechanical model of plastic deformation in semicrystalline polymers is based on the role of cavitation and micronecking [3, 4, 20, 21, 80]. This model was elaborated by Peterlin and coworkers and assumes that plastic

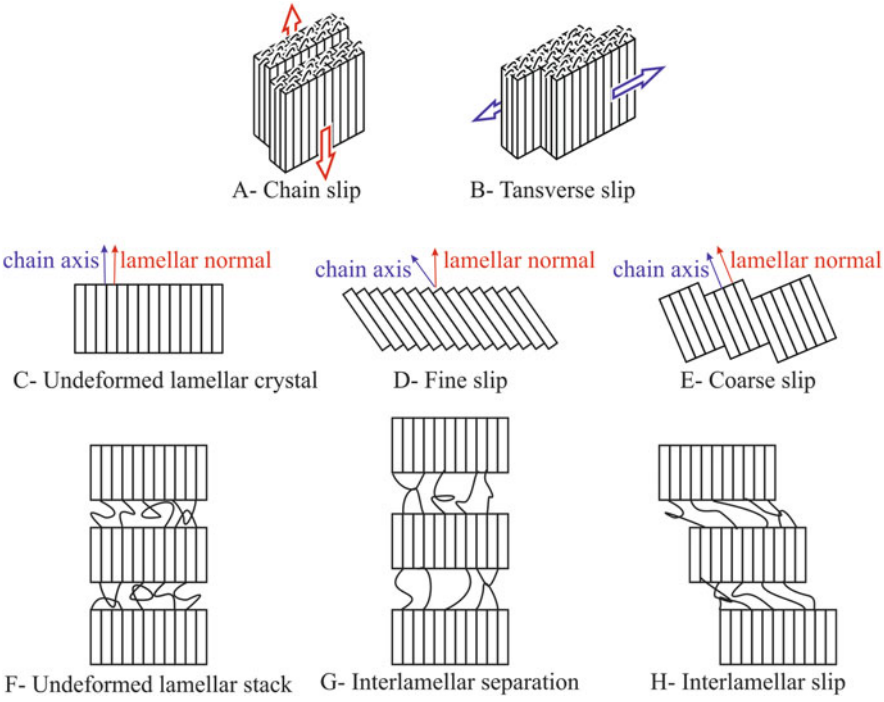

Fig. 1 (**A**, **B**) Two types of crystallographic slip in macromolecular crystals: chain slip (longitudinal) (**A**) and transverse slip (**B**) [6, 25]. Regular chain folds connect adjacent stems in the crystal. *Arrows* denote the direction of the chain translation. Slip occurs parallel to chain fold. (**C**–**E**) Deformation modes of lamellar crystals [32]: undeformed crystal (**C**), models of fine chain slip (**D**), and coarse chain slip (**E**). The orientation of chain axes and the vector normal to lamellar surface are indicated. (**F**–**H**) Deformation modes of the amorphous phase: undeformed stack (**F**), interlamellar separation mode (**G**), and interlamellar slip (shear) (**H**). In **G**, **H** only the chains bridging adjacent lamellar crystals are drawn

yielding is a result of the shearing of crystalline lamellae followed by their simultaneous fragmentation into crystal blocks [20, 21, 81]. In practice, the initial lamellar stacks inside the initial isotropic spherulites transform into fibrillar entities during stretching through formation of micronecks, which are generated at microcrack boundaries. Upon fragmentation of the lamellar blocks through chain unfolding, the blocks become oriented with chain axes in the stretching direction, originating microfibrils that are characterized by alternation of crystalline and amorphous regions [20, 21]. The basic mechanism for formation of micronecks is cavitation, because cavities remove mechanical constraints on block rotations. Therefore, cavitation and micronecking constitute the basic steps of Peterlin's micromechanical model [20, 21]. Successive studies have shown that morphological transformation from initial isotropic structures into microfibrils by plastic deformation can also take place without formation of cavities or microvoids [7, 32, 82, 83]. This, for instance, occurs in the regime of plane-strain or uniaxial

compression [84]. Therefore, cavitation is merely a side effect produced by particular deformation modes and is not essential for the plastic deformation process and related transformation of polymer morphology [84]. Moreover, Peterlin's model completely neglects crystallographic slip processes, and although it describes well the effect of tensile drawing, it fails completely for other deformation modes such as compression or plane-strain [7, 84]. By contrast, the crystallographic approach is more general and can explain the full deformation sequence in any deformation mode, without invoking any catastrophic events such as micronecking, melting–recrystallization transformation, or cavitation [1, 2, 5–8].

According to a generalized view, the mechanisms that govern the process of tensile deformation of semicrystalline polymers at low and moderate deformations appear strain controlled, rather than stress controlled [33, 34, 66, 67, 85–88]. Within this scheme, the amorphous phase also plays a key role because it participates in the plastic flow of a polymer at any deformation, starting from the yield point, as a result of the high degree of interconnection between crystals and amorphous phase. This connectivity is ensured by chains crossing the crystal–amorphous interphase and bridging adjacent lamellae, either through tie chains or entanglements created by chains emanating from a crystal that re-enter into the same crystal, after passage through a portion of the adjoining amorphous layer (Fig. 1F) [46, 85]. The principal deformation modes of the amorphous phase are interlamellar shear and interlamellar separation (Fig. 1G, H).

In general, the contribution of the amorphous phase to plastic deformation at yield is small and the contribution of the amorphous phase becomes predominant only at large deformations, that is, at deformations corresponding to almost complete lamellar fragmentation and consequent transformation of the spherulitic morphology into fibrillar morphology. In principle, deformation of the intralamellar amorphous regions at temperatures higher than the glass transition is largely recoverable, especially at low deformation. This is a result of the rubbery state of the amorphous phase and the high degree of connectivity of the amorphous phase with the crystalline scaffold, which hampers viscous flow. Moreover, because of this connectivity and the intrinsic incompressibility of the amorphous phase, there is an intrinsic difficulty for the amorphous phase to compensate the deformation along a given direction with shape distortions in the transversal section, as required for volume conservation of the rubbery state [5–7, 14–19]. A direct consequence of this difficulty is that, after yielding, there can be formation of microvoids, lamellar bending (kinking), and consequent stack rotation because these modes cause relaxation of the local strain and prevent scission of the tie chains [85–88]. In all cases, at both large and small deformations, the chains involved in the bridges between adjacent crystals act as efficient stress transmitters [5, 7, 10, 89, 90] that facilitate macroscopic deformation of the sample, up to breaking at large deformations.

More precisely, for deformation temperatures T_{def} higher than the glass transition T_g and immediately after the elastic regime, the plastic deformation of a semicrystalline polymer starts with small distortions of the amorphous portions of the chains located between crystals. The compliant amorphous regions are expected

to deform more easily than the crystals, according to the modes depicted in Fig. 1D, E [2–7]. However, this deformation is quickly exhausted because of the high increase in local stress. This stress is transferred to adjacent crystals. Yield starts as soon as local stress reaches the level of critical resolved shear stress for the easiest slip system, so that the crystals become involved in plastic flow [2–7, 25–28]. From this point on, the plastic deformation of crystals begins to control the whole deformation kinetics of the sample, whereas the amorphous layers respond trough continuous adjustments of their conformation [2–7, 25, 27, 62–65]. With increased deformation, the conformation of amorphous chains eventually becomes so taut that collective movements of the crystals are induced, including fragmentation of lamellae into blocks, complete destruction of the initial morphology, and rotation of the stacks [62–65, 85–88]. Therefore, the entire deformation process involves the simultaneous, combined deformation of amorphous and crystalline components. Crystallographic control dominates until the breakdown of crystallites [32–34, 66, 67, 83, 91]. Afterwards, strain hardening may intervene at large deformations prior to breaking [5–7, 26]. Strain hardening is related to the orientational hardening of the amorphous phase and, to a lesser extent, to reorientation of crystals as a result of crystal slip in the late stages of the deformation process. Along the true stress–true strain curves of polymeric materials, the compliance changes at well-defined points corresponding to changes in crystalline morphology and in the relative response of a material in terms of plastic versus elastic deformation [33, 34, 66, 67, 85–87]. These critical points correspond to:

(A) The onset of isolated inter- and intralamellar slip processes after the initial Hooke's elastic range
(B) Change into a collective activity of slip motions of crystal blocks at the point of maximum curvature of the true stress–strain curve
(C) The beginning of destruction of crystal blocks followed by re-crystallization with formation of fibrils
(D) The beginning of disentanglement of the amorphous network or strain hardening as a result of stretching of the amorphous entangled network at high deformations

The values of the strains at critical points A, B, and C are invariant, for each class of polymer, with variation in crystallinity, temperature, strain rate, and crystal thickness [33, 34, 66, 67, 85–87]. In contrast to the strain, stresses at the critical points vary with deformation rate, and present larger values for higher crystallinities and lower values for higher temperatures. These observations comply well with the general assumption that the strain is homogeneously distributed in semicrystalline polymers, whereas the stress is not [48–52, 68, 69]. At low stresses or strains, the forces transmitted by the interconnected crystallites dominate, whereas at high strains the rubber-like network forces are superior [68, 69].

The yield point in engineering stretching experiments is always located a little above point B [85–87]. The position of the critical strain at point C, at which the critical stress that starts destruction of the crystal blocks is achieved, depends on the interplay between the entanglement density of the amorphous phase and the

intrinsic stability of crystals [33, 34, 49–52, 66, 67, 85–87]. A higher entanglement density implies that a higher stress is generated when the sample is stretched. The more stable the crystallites, the higher the stress needed for their destruction [49–52].

Within the framework of the crystallographic approach, models for quantitative predictions of the yield stress of semicrystalline polymers have been developed, based on the assumption that yielding involves thermal activation of screw dislocation with the Burgers vector parallel to the chain axis (vide infra) [25, 31, 68, 69, 82, 92–94]. In the resultant model of thermal activation of dislocation, the free energy required to nucleate a dislocation within the crystalline region has been correlated with considerable success to the measured yield stress of various samples of polyethylene (PE) and isotactic polypropylene (iPP) at temperatures higher than T_g [14–19, 60, 67, 71, 92–96]. In particular, it has been found that at a given temperature the stress required to initiate these dislocations depends on the thickness of the crystals, which accounts quite well for the observed dependence of yield stress on crystal thickness for various samples of PE and iPP, regardless of crystallization conditions, degree of crystallinity, and molecular mass. In particular, the critical free energy required to form a screw dislocation and the shear modulus associated with the slip planes of the dislocation can be extracted from this analysis and correlated with crystallographic features of the material [14–19, 60, 67, 71, 92–96].

In this chapter, the yield behaviors of isotactic copolymers of propene with ethylene, 1-butene, 1-pentene, 1-hexene, and 1-octadecene, prepared with different metallocene catalysts [97–106], are analyzed in terms of the crystallographic approach using the dislocation model. The catalysts allow synthesis of copolymers with compositionally uniform chains, uniform distribution of comonomers along the chain, and tailored microstructure [107–110]. Samples with a very small concentration of stereodefects or regiodefects and variable amounts of comonomeric units, or similar concentration of comonomeric units but different concentration of stereo- and regiodefects, have been prepared. Stereodefects (namely, isolated *rr* triads), regiodefects, and different types and concentrations of comonomeric units have different effects on the crystallization of α- and γ-forms of iPP, and on crystallization properties in general. The differences in polymorphism and crystallization properties, in turn, induce differences in mechanical properties. The polymorphism and crystallization properties of these systems depend not only on the concentration of comonomers, which in a random copolymer regulates the average length of the fully (crystallizable) propylene sequences, but also on the different degree of inclusion of these defects (stereo- and regio-irregularities, comonomeric units) in the crystals of α- and γ-forms of iPP. The inclusion of stereo- and regio-irregularities and comonomeric units in the crystal produces point-like defects and an increase in entropy and/or decrease in internal energy and, consequently, influences the relative stability of the crystals [97–106, 111–117]. Therefore, study of the yield behavior of these copolymers allows use of the dislocation model to be extended to a set of samples crystallized under similar conditions but characterized by differences in the degree of crystallinity, lamellar

thickness, polymorphism, and intrinsic flexibility of the chain backbone. The values of these parameters can be finely tailored independently of each other by the type and concentration of defects by simply selecting a different catalyst system. In particular, the present investigation aims at establishing the influence of different degrees of inclusion of point-like defects inside crystals on the parameters of the dislocation model, namely the critical free energy required to form a screw dislocation and the shear modulus associated with the slip planes of the dislocation [25, 92–94]. The final goal is to understand the macroscopic properties of materials at the molecular scale.

2 Experimental Details

The samples selected for this study were iPP homopolymers and propylene-ethylene (iPPEt) [97, 98], propylene-(1-butene) (iPPBu) [97–99], and propylene-(1-hexene) (iPPHe) [98, 105, 106] copolymers prepared at temperatures between 60°C and 70°C with the metallocene catalysts A–C shown in Scheme 1, activated with methylalumoxane (MAO). Samples of propylene-(1-pentene) (iPPPe) [103, 104] and propylene-(1-octadecene) (iPPOc) [102] were prepared at 25°C with catalyst D (see Scheme 1). The three C2-symmetric metallocenes A, C, and D are not completely regioselective, but highly isoselective [107, 108, 110]. The C1-symmetric metallocene B is fully regioselective but not perfectly isoselective [109]. The MAO-activated metallocenes A and B for the synthesis of iPPEt and iPPBu copolymers were supported on spherical SiO_2 particles, or on porous polyethylene or polypropylene particles, following a Basell proprietary technology [118].

All samples are listed in Table 1. The copolymers are designated YZx, where Y is the catalyst (A, B, C, or D) and *x* is the concentration of the comonomeric unit Z (where Z=E, B, P, H, and O stands for ethylene, 1-butene, 1-pentene, 1-hexene, and 1-octadecene, respectively).

The microstructural data of all samples were obtained from ^{13}C NMR analysis (see [97–106] for details). The samples of iPP homopolymer prepared with the catalysts A (iPPA), C, and D (iPPD) are similar. They are highly stereoregular and contain only small amounts of stereoerrors (0.2 and <0.1 mol% of *rr* triad defects in iPPA and iPPD, respectively) and regiodefects caused by secondary 2,1 erythro units (2,1e) (0.8 and 0.2 mol% of 2,1e units in iPPA and iPPD, respectively). The iPP sample prepared with catalyst B is highly regioregular (no 2,1 regiodefects detectable) but less stereoregular, and contains 3.5 mol% *rr* triads [119].

All catalysts produce copolymer samples with microstructures similar to those of the homopolymer samples prepared with the same catalyst, with small oscillations in the concentration of *rr* stereoerrors and 2,1e regiodefects around those of the corresponding iPP (Table 1). In particular, for iPPBu copolymers prepared with the catalyst A the concentration of 2,1e regiodefects decreases with increasing butene

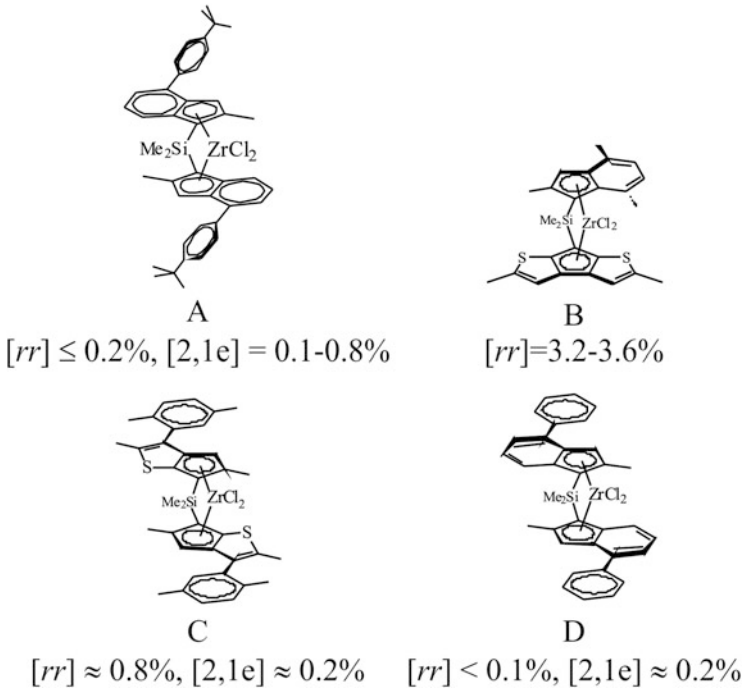

Scheme 1 Structures of metallocene catalysts *A–D* used for synthesis of the samples listed in Table 1

content (Table 1) [97, 98]. For iPPEt and iPPHe copolymers prepared with catalyst A, the content of stereoerrors is not determinable and is assumed to be the same as that found in the corresponding homopolymer iPPA (Table 1) [97, 98, 100, 101]. All the copolymers have a random distribution of comonomers and narrow molecular mass distributions. Details of the NMR analysis are described in the literature [97–106].

The films used for structural and thermal characterization and for mechanical tests were prepared by compression molding. Powder samples were heated at temperatures 20–30°C higher than the melting temperatures between flat brass plates under a press at low pressure and slowly cooled to room temperature by fluxing water in the refrigerating circuit of the press plates. Special care was taken to obtain films of uniform thickness (0.3 mm) and to minimize surface roughness, according to the recommendation of the standard ASTM D-2292-85.

Calorimetric data were collected with a differential scanning calorimeter (DSC) Mettler DSC-30 in a flowing N_2 atmosphere at heating rate of 10°C/min. All samples showed a T_g lower than ≈0°C, which decreased with increasing comonomer concentration and length of the side chains [97–106].

Table 1 Details of iPP homopolymers and various copolymers prepared using different MAO-activated metallocene catalysts

Sample[a]	Catalyst/cocatalyst/carrier[b]	M_w (kg/mol)[c]	M_w/M_n[d]	M_v[e] (kg/mol)	T_m[f] (°C)	Comonomer	Comonomer conc.[g] (mol%)	[*rr*][h] (mol%)	[2,1e][i] (mol%)	ε_{tot}[j] (mol%)
Homopolymers iPP [97, 103]										
iPPA	A/MAO/PE	237	2.2	–	151	–	0	0.2	0.8	1.00
iPPB	B//MAO/PP	247	2.3	–	135	–	0	3.5	0	3.5
iPPD (iPPC)	D//MAO/PP	–	–	680	151	–	0	<0.1	0.2	0.2
Propene-ethylene copolymers iPPEt [97, 98]										
AE0.6	A/MAO/PE	–	–	–	146	Ethylene	0.6	0.2[k]	0.7	1.5
AE4.0	A/MAO/PE	293	2.1	–	130	Ethylene	4.0	0.2[k]	0.6	4.8
AE7.4	A/MAO/PE	289	2.1	–	117	Ethylene	7.4	0.2[k]	0.4	8.0
BE3.6	B/MAO	–	–	–	121	Ethylene	3.6	3.6	0	7.2
BE13.1	B/MAO	193	2.0	–	47, (113)[l]	Ethylene	13.1	3.2	0	16.3
Propene-1-butene copolymers iPPBu [97–99]										
AB1.9	A/MAO/SiO_2	316	2.2	–	144	1-Butene	1.9	<0.1	0.5	2.4
AB4.3	A/MAO/PE	229	2.1	–	137	1-Butene	4.3	<0.1	0.4	4.7
AB8.3	A/MAO/SiO_2	200	2.1	–	130	1-Butene	8.3	<0.1	0.3	8.6
AB13.6	A/MAO/SiO_2	161	2.4	–	115	1-Butene	13.6	<0.1	0.1	13.7
CB12	C/MAO	–	–	165	119	1-Butene	12.0	0.2	0.8	13.0
CB27.6	C/MAO	–	–	182	88	1-Butene	27.6	0.2	0.8	28.6
CB37.3	C/MAO	–	–	177	76	1-Butene	37.3	0.2	0.8	38.3

(continued)

Table 1 (continued)

Sample[a]	Catalyst/cocatalyst/carrier[b]	M_w (kg/mol)[c]	M_w/M_n[d]	M_v[e] (kg/mol)	T_m[f] (°C)	Comonomer	Comonomer conc.[g] (mol%)	[*rr*][h] (mol%)	[2,1e][i] (mol%)	ε_{tot}[j] (mol%)
Propene-1-pentene copolymers iPPPe [103, 104]										
DP3.2	D/MAO	428	1.8	–	126	1-Pentene	3.2	<0.1	0.2	3.4
DP5.3	D/MAO	347	2	–	105, (51)[l]	1-Pentene	5.3	<0.1	0.2	5.5
DP8.8	D/MAO	279	2	–	85, (51)[l]	1-Pentene	8.8	<0.1	0.2	9.0
DP11.0	D/MAO	–	–	–	68, (50)[l]	1-Pentene	11.0	<0.1	0.2	11.2
Propene-1-hexene copolymers iPPHe [100, 101, 105, 106]										
AH2.0	A/MAO	122	2.4	–	127	1-Hexene	2.0	0.2	0.2	2.4
AH3.7	A/MAO	333	2.0	–	116	1-Hexene	3.7	0.2	0.2	4.1
AH6.8	A/MAO	239	2.2	–	96	1-Hexene	6.8	0.2	0.1	7.1
AH11.2	A/MAO	266	1.9	–	70	1-Hexene	11.2	0.2	0.1	11.5
Propene-1-octadecene copolymers iPPOc [102][m]										
DO1	D/MAO	–	–	–	139	1-Octadecene	1	<0.1	0.2	1.2
DO2.2	D/MAO	–	–	–	117	1-Octadecene	2.2	<0.1	0.2	2.4
DO4.8	D/MAO	–	–	–	93	1-Octadecene	4.8	<0.1	0.2	5.0

DO6.0	D/MAO	–	–	–	85	1-Octadecene	6.0	<0.1	0.2	6.2
DO7.5	D/MAO	–	–	–	55, 69[n]	1-Octadecene	7.5	<0.1	0.2	7.7

[a]iPP homopolymers (iPPA, iPPB, and iPPD) and iPPEt, iPPBu, iPPPe, iPPHe, and iPPOc copolymers were prepared with the MAO-activated metallocenes A–D shown in Scheme 1. Sample designations are of the form YZx, where Y is the catalyst (A, B, C, or D) and *x* is the concentration of the comonomeric unit Z (where Z=E, B, P, H, and O stands for ethylene, 1-butene, 1-pentene, 1-hexene, and 1-octadecene, respectively)
[b]*PE* polyethylene, *PP* polypropylene
[c]Mass-average molecular mass (M_w) was obtained by GPC
[d]Polydispersity M_w/M_n. SEC curves show molecular mass distributions for all samples of around 2.0
[e]Values of viscosity average-molecular masses (M_v) were obtained from values of the intrinsic viscosities [η]
[f]Melting temperature (T_m) of compression-molded samples crystallized from the melt by slow cooling to room temperature while fluxing cold water in the refrigerating circuit of the press plates
[g]Concentration of comonomeric units (mol%) determined from solution ^{13}C NMR analysis
[h]Percentage content of primary stereoerrors over all monomer units, $[rr] = [mrrm] + [mrrr]$. For copolymers samples prepared with A, C, or D where the content of stereoerrors is not determinable, the quantity [*rr*] is assumed to be the same as that found in the homopolymers iPPA and iPPD
[i]Concentration of secondary 2,1-erythro units [2,1e]. Secondary insertions 2,1 are only of the erythro type, and their amount is normalized over all monomer units. For iPPEt copolymers, [2,1e] is the sole concentration of isolated secondary 2,1-erythro units (PSP, P = propylene, S = secondary 2,1 propylene unit)
[j]Total concentration of defects (ε_{tot})
[k]Content of stereoerrors was not determinable and was assumed to be the same as that found in the corresponding homopolymer iPPA
[l]Temperature of a low melting endothermic peak
[m]Samples were fractioned with boiling ethoxyethane to remove unreacted 1-octadecene comonomer
[n]Sample shows a double melting endotherm

X-ray diffraction patterns (WAXS) were obtained at room temperature with Ni-filtered CuKα radiation ($\lambda = 1.5418$ Å). The powder profiles were obtained using a Philips diffractometer with continuous scans of the 2θ angle and scanning rate of 0.02°/s.

The indices of crystallinity (x_c, relative error 10%) were evaluated from the X-ray powder diffraction profiles from the ratio between the crystalline diffraction area (A_c) and the total area of the diffraction profile (A_t), $x_c = A_c/A_t$. The crystalline diffraction area was obtained from the total area of the diffraction profile by subtracting the amorphous halo. The procedure used for evaluation of the amorphous halo for each sample and for the subtraction is the same as previously published [97–106].

Small angle X-ray scattering (SAXS) data for compression-molded films were collected at room temperature using a Kratky compact camera SAXSess (Anton Paar, Graz, Austria) in the slit collimation configuration, attached to a conventional X-ray source (CuKα, wavelength 1.5418 Å). The scattered radiation was recorded on a BAS-MS imaging plate (Fujifilm) and processed with a digital imaging reader (Fujibas 1800). The range of scattering vector modulus, $0.1\ \text{nm}^{-1} \le q \le 2\ \text{nm}^{-1}$, where $q = (4\pi\sin\theta/\lambda)$ and 2θ is the scattering angle, was analyzed. After subtraction for dark current, the empty sample holder, and a constant background caused by thermal density fluctuations, the slit smeared data were de-convoluted with the primary-beam intensity distribution using the SAXSquant 2.0 software to obtain the corresponding pinhole scattering (desmeared) intensity distribution. The constant value of intensity approximating the background I_{back} was found by fitting the smeared SAXS intensity curve in the range $2 < q < 4\ \text{nm}^{-1}$ [$I(q_{high})$] with the function [120, 121]:

$$I(q_{high}) = I_{back} + bq^{-3} \tag{1}$$

where I_{back} and b are fitting parameters. The average value of the long period L was calculated as $L \approx 2\pi/q^*$, where q^* is the q value corresponding to the maximum in the Lorentz-corrected intensity (i.e., the SAXS intensity multiplied by q^2/π). Crystal thickness l_c was then calculated by $l_c \approx x_c L$, where x_c corresponds to the degree of crystallinity, as evaluated from WAXS profiles. The thickness of amorphous layers, l_a, was evaluated as $l_a = L - l_c$. In practice, we used the mass fraction of the crystalline phase derived from WAXS analysis instead of the volume fraction, because the density of amorphous copolymers was not directly determined. Therefore, even though the calculated values of l_a and l_c are affected by an absolute error, they are of significance in comparing the properties of the different samples. It is worth noting that the average values of the long period and lamellar thickness (and thickness of amorphous layers) evaluated using the one-dimensional correlation function [120] or the interface distribution function [121] would give similar results to those evaluated directly from the q values at the maximum of the Lorentz-corrected scattering intensity.

Mechanical tests were performed at room temperature on compression-molded films with a universal testing machine Zwicki (Zwick/Roell), following the standard test method for tensile properties of thin plastic sheeting (ASTM D882-83). Rectangular specimens 10 mm long, 5 mm wide, and 0.3 mm thick were stretched to the break point or to a given deformation $\varepsilon = [(L_f - L_0)/L_0]100$, where L_0 and L_f are the initial and final lengths of the specimen, respectively. Two benchmarks were placed on the test specimens and used to check the local elongation versus the nominal elongation measured from the grip-to-grip distance. In mechanical tests, the ratio between the drawing rate and the initial length was fixed at 10 mm/(mm min). The stress–strain curves and the reported values of the mechanical parameters were averaged over at least five independent experiments.

3 Structural Analysis and Thermal Behavior

The crystallization behavior of isotactic copolymers of propene with ethylene, butene, pentene, hexene, and octadecene synthesized with single-center metallocene catalysts has been extensively studied [97–106, 111–117], and compared with that of the corresponding homopolymer iPP produced with the same catalyst system. Single-center metallocene catalysts allow perfect control over the chain microstructure [122]. Thus, iPP-based homo- and copolymer samples characterized by different kinds and amounts of defects along the chain can be produced while maintaining tight control over molecular mass, molecular mass distribution (with polydispersity index close to two), and uniform inter- and intrachain distributions of the defects. Study of these systems has allowed isolation of the different influences of each kind of defect, namely stereodefects (isolated *rr* triads), regiodefects (e.g., secondary 2,1 insertions of monomeric units), and comonomeric units, on the crystallization of α- and γ-forms of iPP.

In particular, it has been shown that chain microstructure strongly influences the polymorphic behavior and physical properties of iPP [40, 41, 97, 100, 111, 114, 119, 123–130]. Samples characterized by chains containing microstructural defects (stereodefects and regiodefects) and/or comonomeric units, generated by different catalysts, crystallize as a mixture of the α- and γ-forms (Fig. 2A, B) [40, 41, 97, 100, 111, 114, 119, 123–130]. In general, formation of the γ-form seems favored by the presence of these defects [40, 41, 97, 100, 111, 114, 119, 123–130]. However, each kind of defect influences the crystallization of α- and/or γ-forms in a different way according to different mechanisms. A rational and unified picture of the complex polymorphism of these systems [97, 100, 102] has been achieved and the general rules controlling the polymorphism of iPP in defective samples have been identified.

The first important parameter that influences the crystallization of α- and γ-forms of iPP corresponds to the average length of the regular isotactic propylene sequences [40, 41, 119, 123–130]. Short regular isotactic sequences generally favor

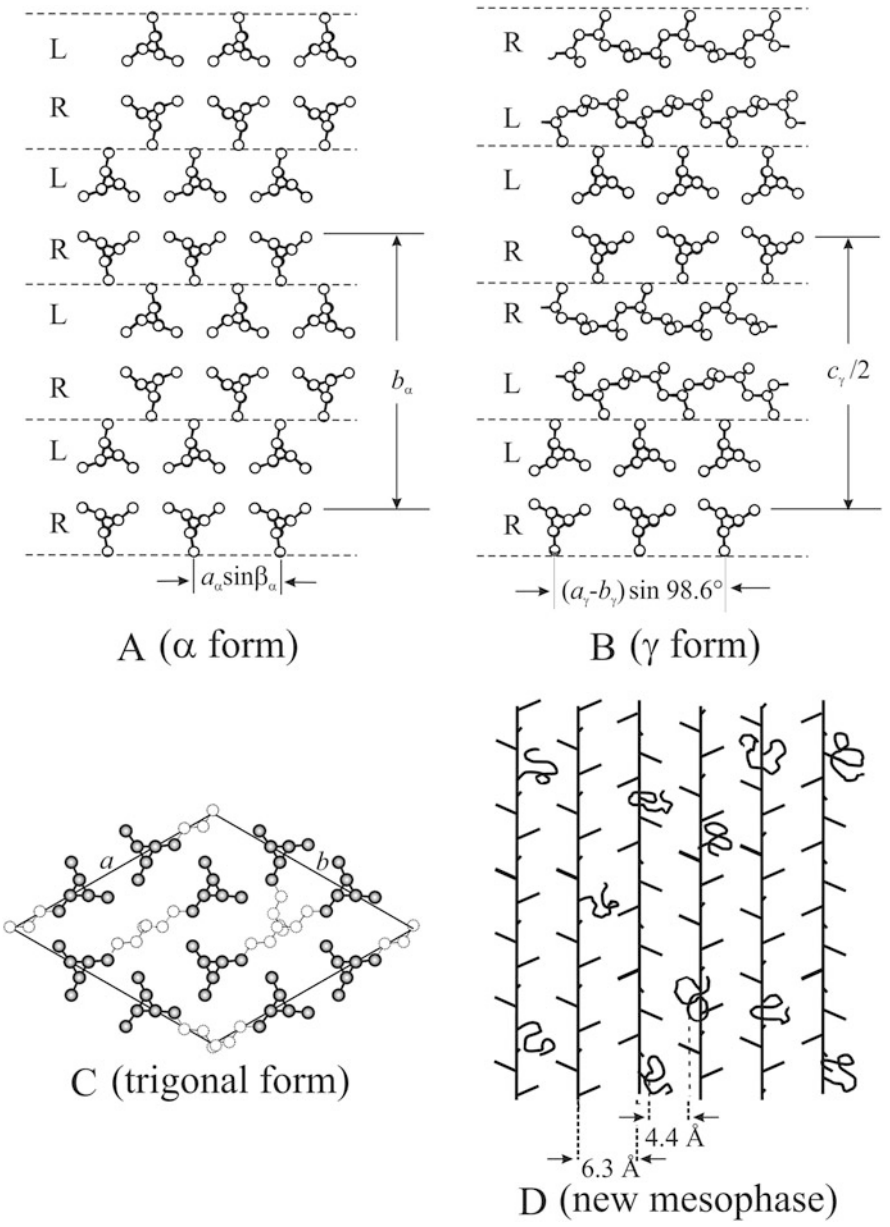

Fig. 2 Structural models of α-form (**A**) and γ-form (**B**) of isotactic polypropylene. (**C**) Trigonal form of isotactic copolymers of propene with 1-pentene and 1-hexene containing pentene concentrations higher than 10 mol% and hexene concentrations higher than 15–16 mol% [100, 101, 103, 104]. The structural model of iPPHe copolymers in the trigonal form is shown as an example. The lateral butyl groups of 1-hexene units are statistically included in the unit cell with occupancy factor close to the average content of comonomers in the copolymer chain. (**D**) New mesomorphic form of isotactic copolymers of propene with long 1-alkene [102].

crystallization of the γ-form. For metallocene-made homo- and copolymers of propene characterized by random distribution of defects along the chains, the average length of propene crystallizable sequences scales with the reciprocal concentration of defects. Therefore, even a small number of defects shortens the average length of the regular isotactic sequences, reducing the melting temperature and favoring crystallization of the γ-form [40, 41, 119, 123–130]. Because of the non-parallel arrangement of chains in crystals of the γ-form (Fig. 2B), defects are easily accommodated at the lamellar boundaries, with no need for chain folding. By contrast, in the α-form (Fig. 2A) defects are rejected at the fold surface because chain folding is a necessary requisite for crystallization in order to avoid overcrowding at the lamellar surface.

A second remarkable effect that drives the crystallization of α- and/or γ-forms is the possible inclusion of defects in crystals of the two polymorphs [97, 100]. The inclusion effect favors crystallization of the form that better tolerates the defect within its crystalline lattice. Therefore, the two effects can either act synergistically in favoring crystallization in a polymorph, or in competition [97, 100]. In principle, the interruption effect is common to any defect (stereo- and regiodefects and comonomeric units) and always favors crystallization of the γ-form. The inclusion effect produces point-like defects inside the crystals, which may influence the conformational and packing energy of α- and γ-forms to equal or different extents. The final crystalline form obtained upon crystallization depends on the effective level of disturbance of the defects inside the crystalline lattice, which, in the case of copolymers, is related to the size of the comonomeric units [97, 100, 131].

A third peculiar effect has also been demonstrated in the case of some copolymers that, above a threshold concentration of comonomeric units, tend to crystallize in a polymorphic form that is different to both α- and γ-forms [100–106]. Crystallization into the new polymorph is driven by the easy inclusion of comonomers inside crystals of the new form. The process is driven by an increase in entropy and density [103–106, 132–140] or by kinetic factors [102]. In other words, crystallization of the new polymorph is competitive with crystallization of the α-form (expected on the basis of the inclusion effect) and/or the γ-form (expected on the basis of the interruption effect). We call this effect the "competitive crystallization effect."

It has been shown that iPP homopolymer samples with different concentrations of *rr* defects [40, 41, 119, 123–130] and samples of iPPEt and iPPBu copolymers [97, 111] crystallize from the melt as mixtures of the α- and γ-forms. The amount of γ-form increases with increasing crystallization temperature, ethylene concentration, and content of *rr* stereodefects. By contrast, in iPPBu copolymers, the amount of the γ-form first increases, then decreases for concentrations of butene units higher than 10–14 mol% and is always lower than that crystallized in stereodefective iPP and iPPEt copolymers [97, 99]. Therefore, *rr* stereodefects and ethylene units favor the crystallization of the γ-form, whereas butene units favor crystallization of the α- and γ-forms at high and low concentrations, respectively.

These data have been rationalized by resorting to the combined effect of interruption and inclusion [97, 119]. First, it has been shown that in stereodefective

iPP, iPPEt, and iPPBu copolymers, different proportions of *rr* defects, ethylene, and butene are included in crystals of the α- and γ-forms [112, 113]. On the one hand, the interruption effect favors crystallization of the γ-form. On the other hand, the inclusion effect also comes into play and the two effects act simultaneously, with one prevailing over the other depending on the compatibility of the different defects within the crystalline lattices of the different polymorphs.

Ethylene and *rr* stereodefects are included in crystals of both α- and γ-forms but are more easily included in crystals of the γ-form [97]. In iPPEt copolymers and in stereodefective iPP samples, the effects of crystal inclusion and shortening the regular propylene sequences produce the same result of favoring crystallization of the γ-form [97, 119].

In the case of iPPBu copolymers, butene units are included without differentiation between crystals of the α- and γ-forms, but are more easily included in the α-form at high concentrations [97]. At low butene concentrations (< 10 mol%), the effect of shortening the length of regular isotactic propylene sequences prevails and induces crystallization of the γ-form. Hence, at low concentration of butene units (for average propene sequences of 10–100 monomeric units), the relative amount of γ-form increases with increasing butene concentration [97]. For butene concentrations higher than 10 mol%, the effect of inclusion of butene units in crystals of the α-form prevails over the interruption effect [97]. As a consequence, the relative amount of γ-form decreases and iPPBu samples with butene concentrations higher than 20–30 mol% always crystallize in the pure α-form, crystallization of the γ-form being completely inhibited.

It has been shown that the crystallization of iPPPe [103, 104] and iPPHe [100, 105, 106] copolymers from the melt produces mixtures of α- and γ-forms at low pentene or hexene concentrations. For comonomer concentrations higher than a threshold, they crystallize almost completely into the α-form. Further increase in comonomer content produces crystallization into the trigonal form of iPP [103, 104, 132–140] (Fig. 2C). This is a result of the high inclusion, at high concentrations, of pentene and/or hexene units into crystals of the α-form, driven by density increase, favoring crystallization of the α-form instead of the γ-form [100, 103–106]. Therefore, the inclusion effect prevails at these comonomer concentrations. The interruption effect becomes efficient in promoting crystallization of the γ-form only at very low concentrations of pentene and/or hexene (2–3 mol%) [100, 103–106]. The trigonal form does not crystallize by cooling the melt but crystallizes from the amorphous state by cold-crystallization or, for samples with high pentene or hexene concentration, by aging amorphous samples at room temperature [100, 103, 104, 132–140]. The hexene or pentene units are included in crystals of the trigonal form and, at low concentration, also in crystals of the α-form, producing an increase in the unit cell dimensions. The change in crystallization habit from monoclinic into trigonal, for pentene concentrations higher than 10 mol% and hexene concentrations higher than 15–16 mol%, allows incorporation of higher amounts of monomer in crystals of the trigonal form than in the α-form, and produces an increase in entropy. Therefore, at high pentene/hexene concentration, competitive crystallization of the trigonal form prevails.

In the case of iPPOc copolymers, octadecene units are completely excluded from the crystals of α- and γ-forms, and only the interruption effect plays a role [102]. These systems crystallize as mixtures of α- and γ-forms for low octadecene concentrations, even though the relative amount of γ-form is low, probably because of kinetics factors and/or the intrinsic tendency of long side chains to favor formation of chain-folded lamellae of the α-form to alleviate steric hindrance. At octadecene concentrations above 7–8 mol%, the α-form is also destabilized and samples crystallize from the melt into a new mesomorphic form [102] (Fig. 2D). This mesophase is different from the quenched mesomorphic form of iPP homopolymer [141]. It is characterized by parallel chains in 3/1 helical conformation packed at average interchain distances of about 6 Å, defined by self-organization of the flexible side groups and high degree of disorder in the lateral packing of chains [102] (Fig. 2D). Therefore, at high octadecene concentrations, the competitive crystallization effect prevails, leading to formation of the new mesophase instead of α- and/or γ-forms, probably because the crystallization kinetics of the normal α- and/or γ-forms become too slow.

It is worth noting that the crystallization conditions (cooling rate, maximum temperature achieved in the melt, and maximum time that the sample is left at that temperature) can have a strong impact on the resulting structural and morphological features and on the optical and mechanical properties of isotactic copolymers of propene [142–148]. This paper focuses on isotactic copolymers of propene crystallizing from the melt essentially in α- and/or γ-forms, using identical crystallization conditions, as described in "Experimental Details." Samples (Table 1) were selected to probe the effect on yield behavior of inclusion/exclusion of comonomeric units in crystals of the two forms. The X-ray powder diffraction profiles of the compression-molded samples are reported in Fig. 3.

All iPP homopolymer samples crystallize from melt in the α-form. This is indicated by presence of the $(130)_{\alpha}$ reflection at $2\theta \approx 18.6^{\circ}$ of the α-form [149, 150] and absence or negligible intensity of the $(117)_{\gamma}$ reflection at $2\theta \approx 20.1^{\circ}$ of the γ-form [151, 152], as shown by the X-ray powder diffraction profiles in Fig. 3A (curves a, e) and Fig. 3C (curve a).

The iPPEt copolymers crystallize from the melt as mixtures of α- and γ-forms of iPP (Fig. 3A). The relative amount of crystals of the γ-form increases with increasing concentration of comonomers, as indicated by the increase in intensity of the $(117)_{\gamma}$ reflection of the γ-form in the diffraction profiles shown in Fig. 3A.

iPPBu copolymers also crystallize from the melt as mixtures of α- and γ-forms (Fig. 3B) but, in contrast to iPPEt systems, the relative amount of γ-form first increases with butene concentrations up to 10–15 mol% (Fig. 3C, curves a–e) then decreases. For butene concentrations of 26–40 mol%, the pure α-form is obtained (Fig. 3B, curves f, g).

In the case of iPPPe and iPPHe samples, small amounts of crystals in the γ-form are obtained only at low concentrations (2–3 mol%) of comonomeric units (Fig. 3C, D, curves b, c). At higher comonomer concentrations, the pure α-form is obtained (Fig. 3C, D, curve d). Partial inclusion of pentene and hexene units is indicated by

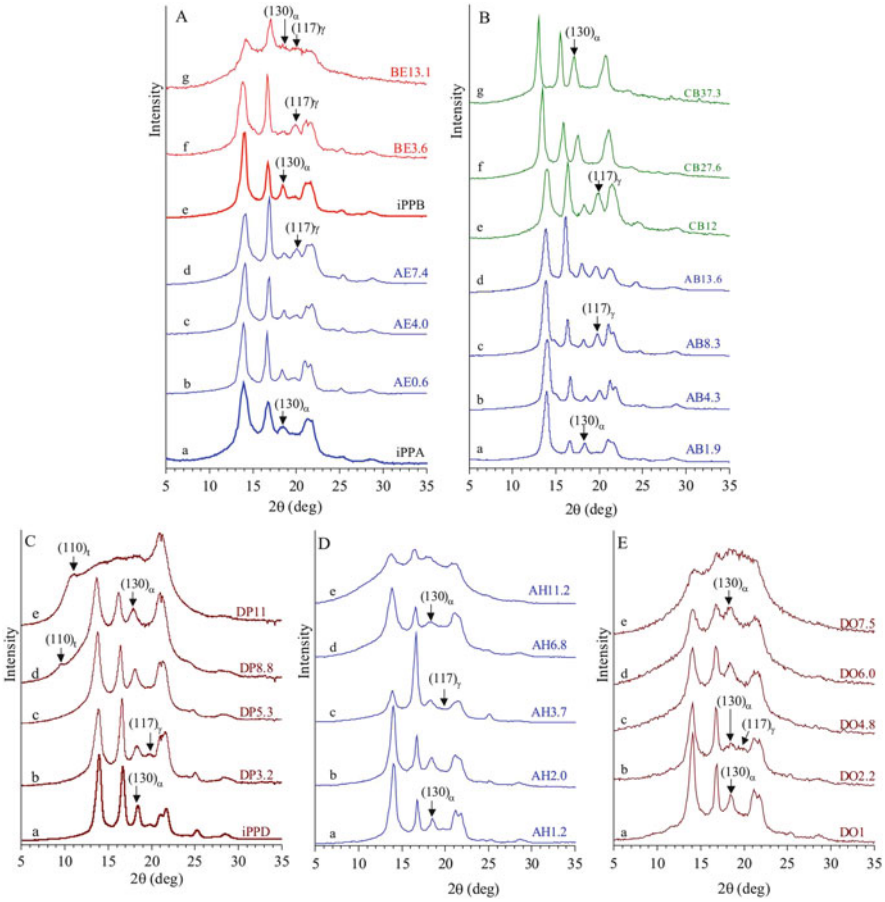

Fig. 3 X-ray powder diffraction profiles of compression-molded samples of the copolymers iPPEt (**A**), iPPBu (**B**), iPPPe (**C**), iPPHe (**D**), and iPPOc (**E**), and of homopolymers iPPA, IPPB, and iPPD prepared with catalysts A–D of Scheme 1. The $(130)_\alpha$ and $(117)_\gamma$ reflections at $2\theta \approx 18.6$ and 20° of the α- and γ-forms of iPP, respectively, and the $(110)_t$ reflection at $2\theta \approx 10°$ of the trigonal form of iPP are indicated

the progressive shift of diffraction peaks toward lower 2θ values with higher comonomer concentrations. With further increase in pentene units, the iPPPe samples crystallize as mixtures of trigonal (Fig. 2C) and α-forms (Fig. 2A) of iPP [100, 101, 103–106]. The relative amount of crystals in the trigonal form is small at a pentene concentration of 8.8 mol% (sample DP8.8; Fig. 3C, curve d), as indicated by the low intensity of the diffraction peak at $2\theta \approx 10°$, corresponding to $(110)_t$ reflection of the trigonal form of iPP [103, 104], and increases at higher pentene concentrations (sample DP11; Fig. 3C, curve e).

Samples of iPPOc crystallize from the melt in the pure α-form (Fig. 3E, curves a, c–e). Crystals of both α- and γ-forms are obtained only for sample DO2.2. However, presence of the new mesophase (Fig. 2D) cannot be excluded [102].

In all cases, the degree of crystallinity (Fig. 4) decreases with comonomer concentration. The decrease is low in the case of iPPBu copolymers and becomes progressively steeper with increasing the size of the comonomeric unit from pentene to octadecene. In particular, in the case of copolymers crystallized with the highly stereoselective but not completely regioselective catalysts A, C, and D it is possible to discern the effect of the presence of comonomeric units on crystallinity and melting temperature. More precisely, the degrees of crystallinity of the copolymers of propene with ethylene (AEx) and pentene (DPx) decrease with the concentration of comonomeric units according to a nearly common trend, in agreement with the fact that ethylene is partially included in the crystals of α- and γ-forms, and pentene in the crystals the of α-form (Fig. 4A). In the case of iPPHe copolymers prepared using catalyst A (AHx), hexene units are partially included in the crystals of the α-form of iPP, and the decrease in crystallinity is only slightly steeper than in iPPPe systems formed using catalyst D (DPx). However, in the case of iPPOc copolymers prepared using catalyst D (DOx), octadecene units are not included at all in the crystals of α- and/or γ-forms because of the high the size of the lateral side chains. As a consequence, the degree of crystallinity rapidly decreases with the concentration of octadecene units and is always lower than for other copolymers of identical concentration (Fig. 4A). In the case of iPPBu copolymers prepared using catalyst A (ABx), which are crystalline in the whole composition range [97–99], the decrease in degree of crystallinity with butene concentration is low (Fig. 4B), in agreement with the good inclusion of the units in the α- and γ-forms of iPP.

In the case of the highly regioregular, less stereoregular, iPPEt copolymers synthesized with catalyst B (BEx), the degree of crystallinity decreases with increasing concentration of ethylene units more rapidly than in the stereoregular and slightly regiodefective samples prepared using catalyst A (AEx) of identical composition, in agreement with the presence of a concentration of *rr* stereodefects of about 3.5 mol%. However, because stereodefects *rr* are also partially included in the α- and γ-forms of iPP and these defects play the same role as ethylene co-units, a plot of degree of crystallinity as a function of the total concentration of defects identifies a common trend for iPPEt copolymers formed using catalysts A or B (Fig. 4B′, inset).

The melting temperature T_m also decreases with increasing concentration of comonomeric units (Fig. 5) but the slope varies according to the comonomer and/or catalyst. Once again, in the case of the regiodefective copolymer samples produced with the catalysts A, C, and D (Fig. 5A), the decrease is least for iPPBu copolymers. This diminution increases for iPPEt copolymers and becomes steeper with increasing size of comonomeric units, following a common trend for iPPPe and iPPHe copolymers, but then drops rapidly for iPPOc systems. Furthermore, in the case of the highly regioregular but stereodefective iPPEt copolymers synthesized with catalyst B, the decrease in melting temperature with increasing total concentration

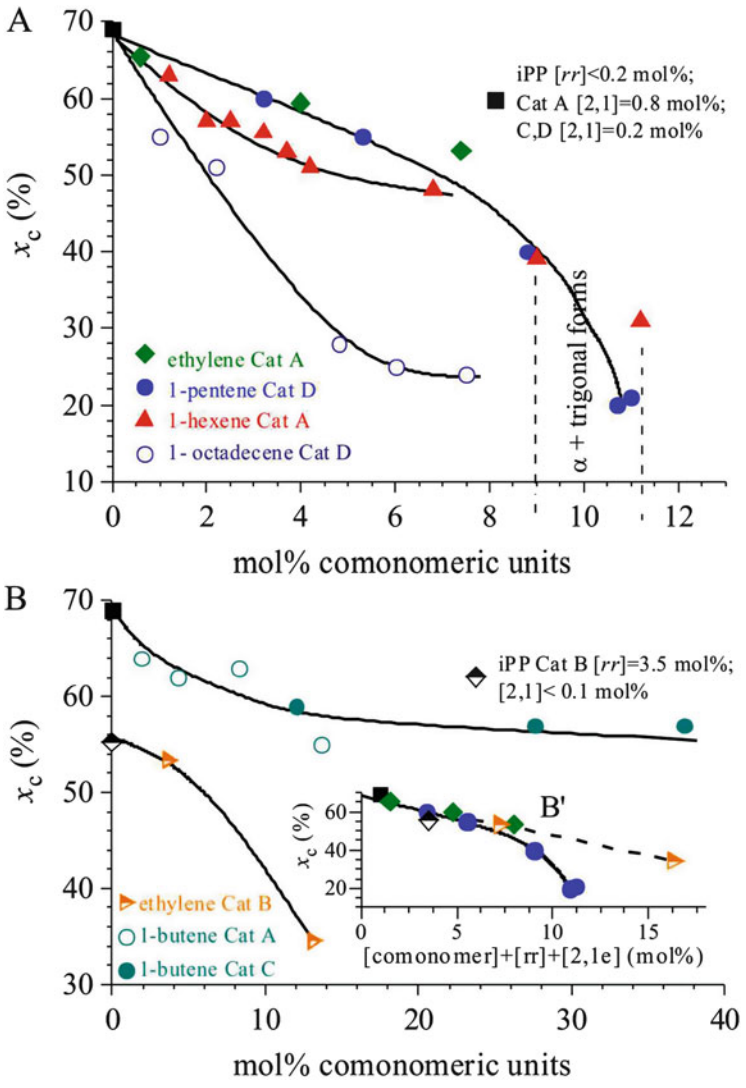

Fig. 4 Degree of crystallinity of iPP homopolymers and iPPEt, iPPBu, iPPPe, iPPHe, and iPPOc copolymer samples prepared with catalysts A–D of Scheme 1, as a function of the concentration of comonomeric units (**A**, **B**) and the total concentration of defects (**B′**, *inset*)

of defects is similar to that for the slightly regioirregular iPPEt copolymers synthesized with catalyst A at similar defect concentration (Fig. 5B).

The Lorentz-corrected SAXS intensity for the compression-molded homo- and copolymer samples listed in Table 1 is shown in Fig. 6. All samples show a broad correlation peak around $q^* \approx 0.5$ nm^{-1} as a result of lamellar stacking. The broadness of the peak increases with increasing comonomer concentration.

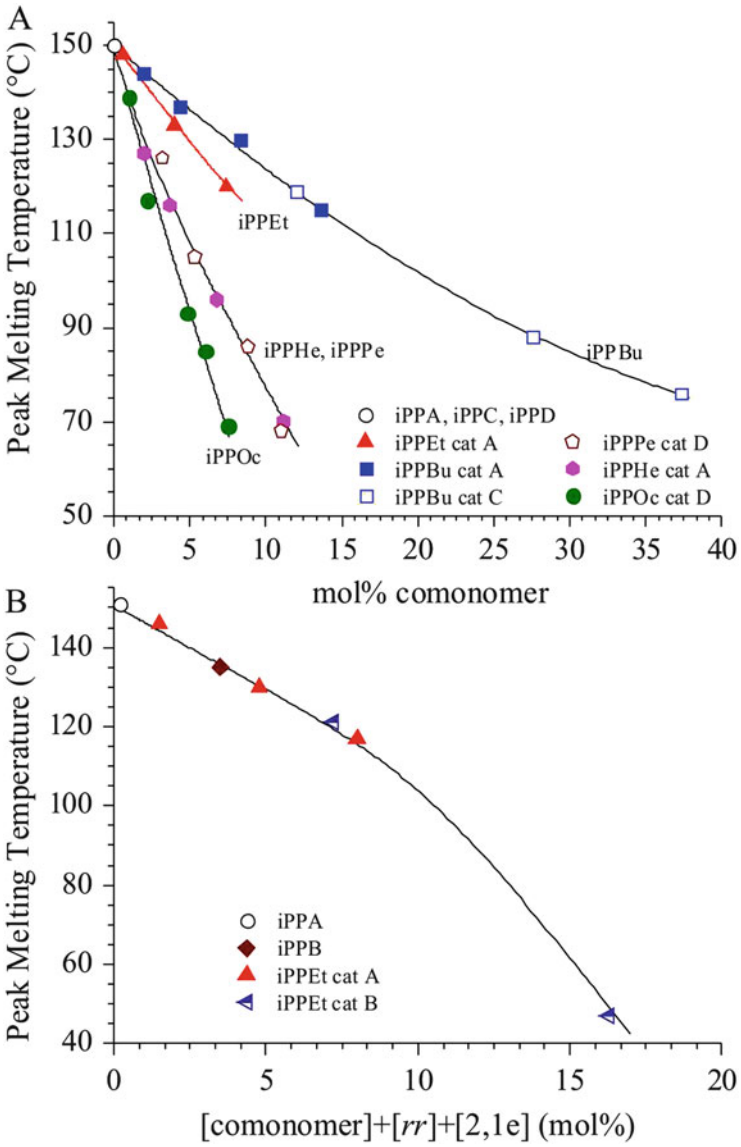

Fig. 5 Melting temperature of iPP homopolymers iPPA, iPPB, iPPC, and iPPD, and of iPPEt, iPPBu, iPPPe, iPPHe, and iPPOc copolymer samples prepared with the catalysts A–D of Scheme 1, as a function of concentration of comonomeric units (**A**) and, in the case of iPPA, iPPB and iPPEt samples, as a function of the total concentration of defects (**B**)

Simultaneously, the SAXS intensity in the background and at low q regions increases, especially for the highly defective samples AB13.6 (Fig. 6B, curve d), DP5.3, DP8.8, and DP11 (Fig. 6C), AH11.2 (Fig. 6D, curve d), and DO6.0 (Fig. 6E,

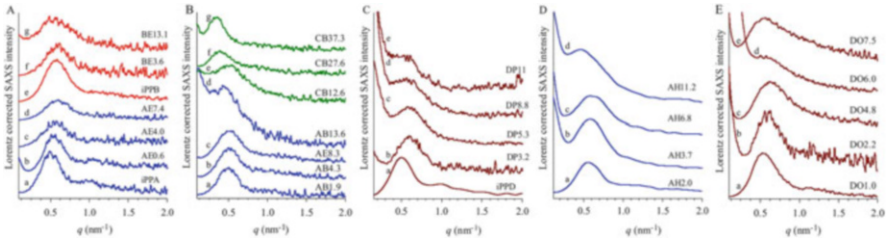

Fig. 6 Lorentz-corrected SAXS intensity of iPP homopolymers and iPPEt (**A**), iPPBu (**B**), iPPPe (**C**), iPPHe (**D**), and iPPOc (**E**) copolymer samples prepared with catalysts A–D of Scheme 1

curve d). The SAXS profiles shown in Fig. 6 can be interpreted in terms of a lamellar morphology, which becomes highly imperfect with increasing comonomer content. Imperfections typically correspond to the formation of distorted lamellae having small lateral dimensions, large distributions of the thicknesses of the crystalline and amorphous layers in the lamellar stacks, formation of short lamellar stacks and/or of more than one population of lamellar stacks with different thicknesses, and, especially for copolymers with a higher concentration of comonomeric units, the presence of single lamellar entities together with a population of periodic arrays of parallel lamellae [153].

The average values of the long spacing L, thickness of the crystalline layer l_c (lamellar thickness), and thickness of amorphous l_a layers for the most representative stacks formed in the compression-molded samples, calculated from the position q^* of the main correlation peak in the SAXS profiles shown in Fig. 5, are compared in Table 2 and Fig. 7. With the exception of iPPBu samples (Fig. 7D), in all cases the lamellar periodicity L is around 11–13 nm. With increasing concentration, L first shows a slight decrease up to a monomer content of 6–8 mol%, then tends to increase at higher comonomer concentration (Fig. 7A–C). The thickness of lamellar crystals tends to decrease, whereas that of amorphous layers tends to increase with increasing comonomer concentration.

Three kinds of behavior can be identified, depending on the degree of inclusion of the comonomeric units in α- and/or γ-forms of iPP. The first kind of behavior corresponds to the case of the isotactic copolymers iPPEt (samples AEx), iPPPe (samples DPx), and iPPHe (samples AHx), produced with the highly stereoselective catalysts A and D, and containing only small amounts of regiodefects. Samples with identical concentrations of comonomeric units develop a lamellar morphology characterized by identical values of the parameters L, l_c, and l_a (Fig. 7A). In these samples, the ethylene, pentene, and hexene units are partially included in the crystals, the decrease in lamellar thickness l_c and increase in thickness of amorphous layers l_a with comonomer concentration are monotonous, whereas the long spacing L first decreases and, then, at higher comonomer concentration, tends to increase slightly. In the case of copolymers iPPEt synthesized with catalyst B (samples BEx) and containing 3.3–3.6 mol% of *rr* stereodefects, the lamellar morphology is characterized by parameters identical to those of samples

Table 2 Comparison of lamellar parameters for iPP homopolymers and various copolymers prepared using different MAO-activated metallocene catalysts

Sample[a]	q^* [b] (nm^{-1})	x_c [c] (%)	L [d] (nm)	l_c [e] (nm)	l_a [f] (nm)	T_m [g] (°C)	Comonomer conc.[h] (mol%)	ε_{tot} [i] (mol%)	σ_y [j] (MPa)	ε_y [k]
Homopolymers iPP										
iPPA	0.51	69	12.32	8.50	3.82	151	0	1.00	–	–
iPPB	0.55	55.3	11.42	6.32	5.11	135	0	3.5	17 ± 2	49 ± 12
iPPD (iPPC)	0.51	69	12.32	8.50	3.82	151	0	0.2		
Propene-ethylene copolymers iPPEt										
AE0.6	0.55	61.4	11.4	7.47	3.95	146	0.6	1.5	–	–
AE4.0	0.57	59.4	11.0	6.55	4.48	130	4.0	4.8	19 ± 5	38 ± 10
AE7.4	0.60	53.1	10.5	5.56	4.91	117	7.4	8.0	17 ± 5	47 ± 10
BE3.6	0.60	53.4	10.5	5.59	4.88	121	3.6	7.2	15 ± 4	49 ± 8
BE13.1	0.56	34.5	11.2	3.87	7.35	47	13.1	16.3	3.9 ± 1	45 ± 9
Propene-1-butene copolymers iPPBu										
AB1.9	0.50	64	12.6	8.04	4.52	144	1.9	2.4	–	–
AB4.3	0.52	62	12.1	7.49	4.59	137	4.3	4.7	18 ± 2	39 ± 4
AB8.3	0.52	63	12.1	7.61	4.47	130	8.3	8.6	17 ± 2	28 ± 3
AB13.6	0.47	55	13.4	7.37	6.03	115	13.6	13.7	14 ± 1	21 ± 2
CB12	0.49	59	12.8	7.56	5.26	119	12.0	13.0	14 ± 1	33 ± 3
CB27.6	0.41	57	15.3	8.74	6.59	88	27.6	28.6	11 ± 1	34 ± 3
CB37.3	0.34	57	18.5	10.5	7.95	76	37.3	38.3	8 ± 1	22 ± 2
Propene-1-pentene copolymers iPPPe										
DP3.2	0.60	60	10.5	6.28	4.19	126	3.2	3.4	22 ± 1	16 ± 2
DP5.3	0.58	55	10.8	5.96	4.88	105	5.3	5.5	13 ± 1	23 ± 2
DP8.8	0.53	40	11.9	4.74	7.11	86	8.8	9.0	8.6 ± 0.5	20 ± 1
DP11	0.52	21	12.1	2.54	9.54	68	11.0	11.2	8.2 ± 0.2	19 ± 1

(continued)

Table 2 (continued)

Sample[a]	q^* [b] (nm^{-1})	x_c [c] (%)	L [d] (nm)	l_c [e] (nm)	l_a [f] (nm)	T_m [g] (°C)	Comonomer conc.[h] (mol%)	ε_{tot} [i] (mol%)	σ_y [j] (MPa)	ε_y [k]
Propene-1-hexene copolymers iPPHe										
AH2.0[c]	0.57	57	11.0	6.28	4.74	127	2.0	2.4	27 ± 3	16 ± 2
AH3.7[c]	0.58	53	10.8	5.74	5.09	116	3.7	4.1	19 ± 1	25 ± 6
AH6.8[c]	0.61	48	10.3	4.94	5.36	96	6.8	7.1	11 ± 1	30 ± 2
AH11.2[c]	0.45	31	14.0	4.33	9.63	70	11.2	11.5	3 ± 1	32 ± 4
Propene-1-octadecene copolymers iPPOc										
DO1	0.55	54	11.4	6.17	5.25	139	1	1.2	20 ± 2	13 ± 2
DO2.2	0.60	51	10.5	5.34	5.13	117	2.2	2.4	13 ± 1	19 ± 2
DO4.8	0.63	28	9.97	2.79	7.18	93	4.8	5.0	7 ± 1	18 ± 2
DO6.0	0.54	25	11.6	2.91	8.73	85	6.0	6.2	5 ± 0.4	18 ± 2
DO7.5	0.57	24	11.0	2.65	8.38	69	7.5	7.7	2.7 ± 0.2	23 ± 2

[a]iPP homopolymers (iPPA, iPPB, iPPD) and iPPEt, iPPBu, iPPPe, iPPHe, and iPPOc copolymers were prepared with the MAO-activated metallocenes A–D of Scheme 1. Sample designations as in Table 1

[b]Position of the correlation peaks (q^*) in the SAXS intensity profiles of Fig. 6

[c]Crystallinity index (x_c) determined from X-ray powder diffraction profiles of Fig. 3

[d]Long spacing (L)

[e]Lamellar thickness (l_c)

[f]Thickness of amorphous layers (l_a)

[g]Peak melting temperature (T_m) of the compression-molded samples crystallized from the melt by slowly cooling to room temperature while fluxing cold water in the refrigerating circuit of press plates

[h]Concentration of comonomeric units (mol%)

[i]Total concentration of defects (ε_{tot})

[j]Stress (σ_y) at yield of compression-molded samples

[k]Strain (σ_y) at yield of compression-molded samples

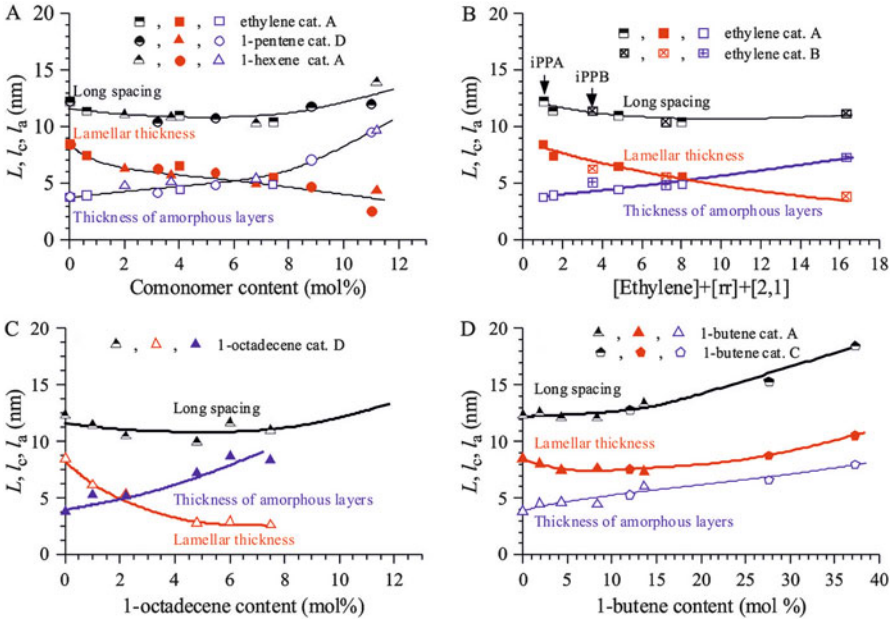

Fig. 7 Long spacing L and the thickness of crystalline l_c and amorphous l_a layers, as calculated from the SAXS profiles shown in Fig. 6, relative to iPPA, iPPB, and iPPD homopolymers and to iPPEt (**A**, **B**), iPPBu (**D**), iPPPe (**A**), iPPHe (**A**) and iPPOc (**C**) copolymer samples prepared with catalysts A–D of Scheme 1. In **B**, the lamellar parameters L, l_c, and l_a of iPPEt copolymers synthesized with catalyst A and containing only 2,1 regiodefects ([2,1e] ≈ 0.4–0.8 mol%) and iPPEt copolymers synthesized with catalyst B and containing only *rr* stereodefects ([*rr*] ≈ 3.2–3.6 mol%) are compared as a function of the total concentration of defects ε_{tot}

synthesized with catalyst A (samples AEx) and having an equal concentration of defects. In particular, as shown in Fig. 7B, plotting L, l_c, and l_a versus the total concentration of defects $\varepsilon_{tot} = [\text{ethylene}] + [rr] + [2,1e]$ for these copolymer samples indentifies a unique trend confirming that *rr* stereodefects play the same role as ethylene co-units in the crystallization behavior of these systems. Also in this case, with increasing the comonomer concentration, we observe a monotonous decrease in lamellar thickness l_c, a monotonous increase in the thickness of amorphous layers l_a, and a slight decrease in the long spacing L. The second kind of behavior corresponds to total inclusion and occurs for the samples of isotactic copolymers iPPBu (Fig. 7D) synthesized with the highly stereoselective catalysts A and C. The easy inclusion of butene units in the crystals of the α-form of iPP always produces crystals with lamellar thickness higher than the lamellar thickness of the other copolymers with identical concentration of units and minor degree of inclusion. With increasing comonomer concentration, the lamellar thickness l_c first decreases, then increases at high butene content, whereas the thickness of the amorphous layers l_a and the long spacing L increase monotonously. The third kind of behavior corresponds to total exclusion and occurs for the isotactic copolymers iPPOc

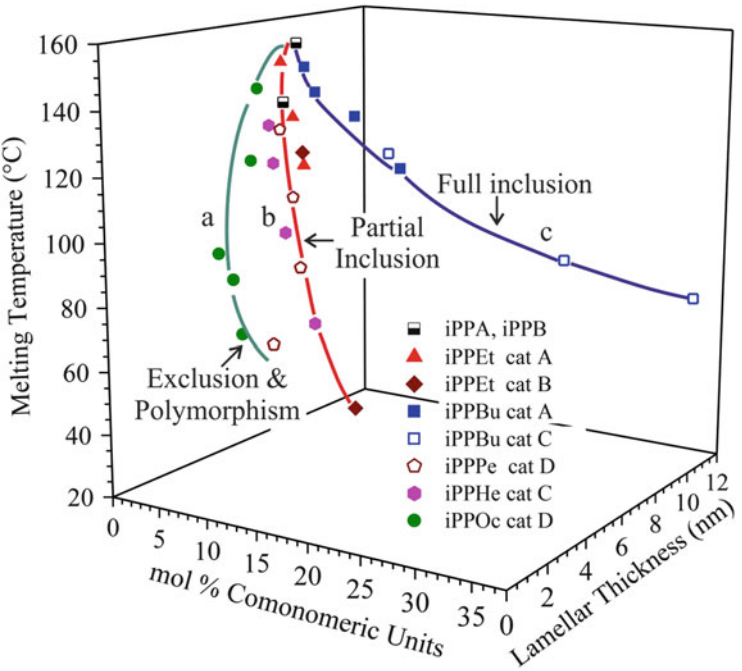

Fig. 8 Melting temperature of iPP homopolymers and iPPEt, iPPBu, iPPPe, iPPHe, and iPPOc copolymer samples prepared with catalysts A–D of Scheme 1, as a function of lamellar thickness and concentration of comonomeric units. For the iPPEt samples prepared with catalyst B, the concentration of *rr* stereodefects (≈3.5 mol%) has been added to the concentration of ethylene units. *Curve a* indicates the trend in the decrease in melting temperature for samples characterized by exclusion of comonomer units from the crystals; *curve b* partial inclusion; *curve c* full inclusion.

(Fig. 7C) synthesized with catalyst D (samples DOx). In this case, the thickness of the lamellar crystals is smaller than that of the copolymers with ethene, butene, pentene, and hexene because the bulky side chains are rejected from the crystals. For the iPPOc copolymers, the decrease in lamellar thickness l_c and increase in thickness of amorphous layers l_a with comonomer concentration are monotonous, whereas the long spacing L decreases only slightly.

From the data of Figs. 5 and 7, it is apparent that parallel to the decrease in melting temperature with comonomer content, the lamellar thickness also decreases. Indeed, the melting temperatures of our copolymers, and semicrystalline polymers in general, depend not only the content of comonomeric units but also on the lamellar thickness [154–158]. A direct correlation between the melting temperature, lamellar thickness, and comonomer content of melt crystallized copolymer samples obtained by compression molding is depicted in Fig. 8. It is apparent that in the case of the copolymers iPPEt, iPPPe, iPPHe, and iPPOc there is a concomitant decrease in melting temperature (Fig. 5) and lamellar thickness (Fig. 7A, B, C and Fig. 8, curves a, b) with increasing the concentration of comonomeric units. By

contrast, in the case of iPPBu copolymers, the melting temperature decreases with increasing butene concentration (Fig. 5), even though the lamellar thickness increases (Fig. 7D and Fig. 8, curve c).

The differences in melting behavior are also common to other systems [154–158] and depend on the different degree of inclusion/exclusion of the comonomeric units in the crystals and/or crystallization into a different polymorph. According to Flory's theory [159] of copolymer crystallization, valid in the limit of strict exclusion, for A/B random copolymers with dilute B units excluded from crystals of A units, the melting temperature of copolymer crystals is lower than that of the A homopolymer exhibiting the same crystal thickness. This is a result of different concentrations of the comonomeric units in the crystals and in the melt in equilibrium. Because the melting temperature T_m is the ratio of the melting enthalpy ΔH_m to the melting entropy ΔS_m ($T_m = \Delta H_m/\Delta S_m$), the presence of B units in the melt in equilibrium with crystals, produces a non-zero mixing entropy contribution to the melting entropy. This contribution increases with increasing concentration of B units in the copolymer, producing a decrease in melting temperature. On the other hand, according to the theory of Sanchez and Eby [160, 161], the melting temperature of an A/B random copolymer is lowered, even in the case of inclusion of B units in the crystals. Even in the limit of uniform inclusion of B units in the crystalline and amorphous regions, which corresponds to zero mixing entropy at melting, the enthalpy penalty for incorporation of B units in the crystals produces a decrease in the melting temperature, whereas lamellar thickness does not decrease.

In our case, the decrease in melting temperature with decrease in lamellar thickness follows a common trend in the case of iPPEt, iPPPe, and iPPHe copolymer samples (Fig. 8, curve b), characterized by partial inclusion of the comonomeric units in the crystals of α- and/or γ-forms of iPP. Moreover, the total exclusion of comonomers from the crystals of α- and/or γ-forms in the case of iPPOc copolymers produces melting depression associated with a major decrease in lamellar thickness (Fig. 8, curve a). Also, in the case of the iPPPe sample with high pentene concentration (DP11.0 containing 11 mol% pentene units), the comonomers are completely excluded from the crystals of α- and/or γ-forms and are better included into the trigonal form [105, 106]. The competitive partial crystallization of the trigonal form causes melting point depression and a decrease in lamellar thickness. In the case of iPPBu copolymers, instead, the total inclusion of butene units in the crystals produces melting depression and no decrease in lamellar thickness (Fig. 8, curve c).

4 Mechanical Properties

The stress–strain curves of melt-crystallized samples of iPP homopolymers and iPPEt, iPPBu, iPPPe, IPPHe, and iPPOc copolymer samples obtained by compression molding are shown in Fig. 9. Only the first portion of the curves (up to 400% deformation) is reported, to put into evidence the yield behavior. It is worth noting that all copolymer samples show high flexibility, toughness, and ductility, with

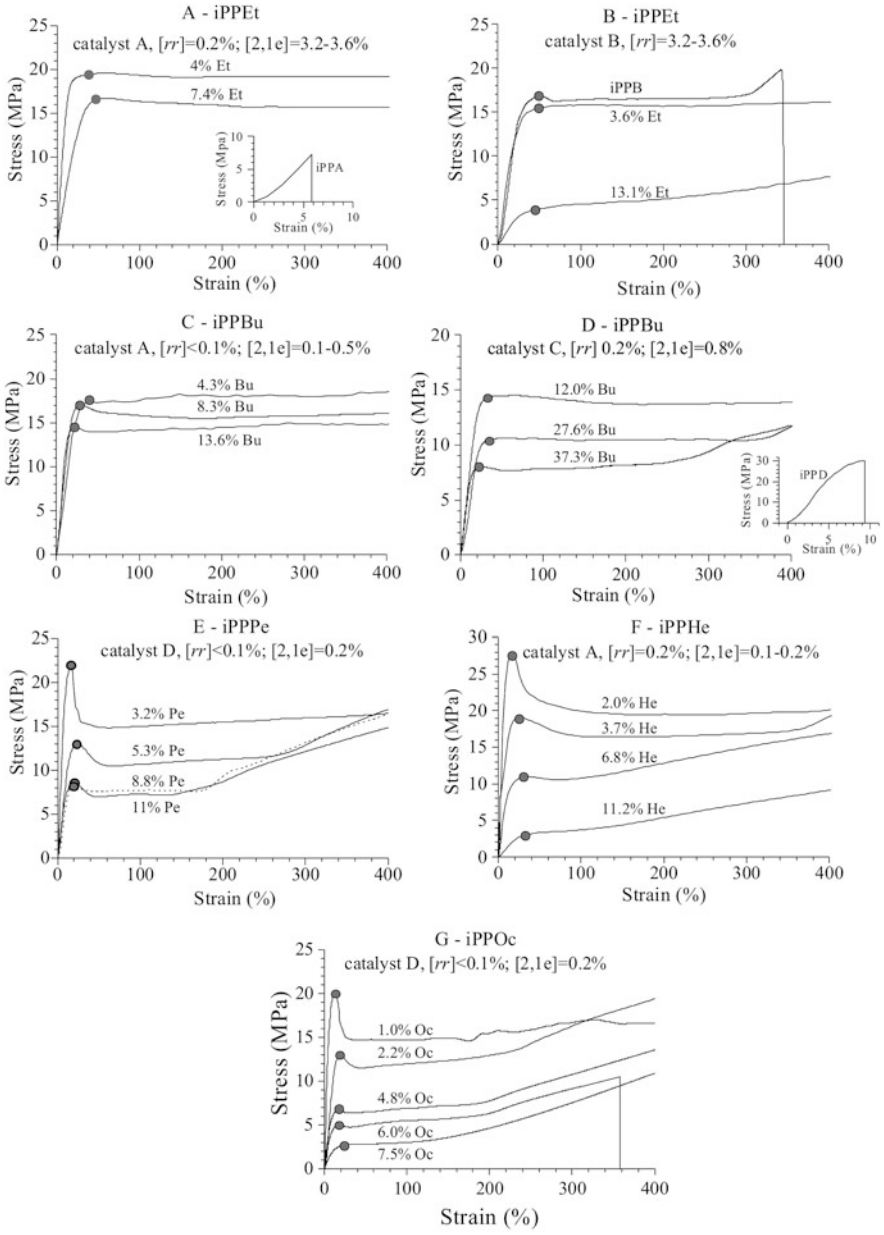

Fig. 9 Stress–strain curves of melt-crystallized films prepared by compression molding of iPP homopolymers iPPA, iPPB, and iPPD and of iPPEt (**A**, **B**), iPPBu (**C**, **D**), iPPPe (**E**), iPPHe (**F**), and iPPOc (**G**) copolymer samples synthesized with catalysts A–D of Scheme 1

deformation at break higher than 300–400% [98, 101, 103]. By contrast, the highly stereoregular iPP samples prepared with catalyst A, C (data not reported), and D of Scheme 1, (iPPA, iPPC, and iPPD) are stiff and fragile materials, as shown in the insets of Fig. 9A, D [40, 41, 127, 128]. Only the highly regioregular, less stereoregular, iPPB sample containing 3.5 mol% *rr* defects shows high flexibility coupled with high toughness and values of deformation at break of about 350% [40, 41, 127] (Fig. 9B).

In all cases, the stress at any strain decreases with increasing concentration of comonomeric units (Fig. 9). Plastic resistance also decreases, as indicated by the values of the yield stress. The stereodefective homopolymer sample iPPB, and the copolymer samples iPPEt and iPPBu show uniform deformation and smooth yield behavior regardless of comonomer concentration (Fig. 9A–D) [98]. By contrast, the highly stereoregular copolymer samples with side chains longer than the ethyl group (iPPPe, iPPHe, and iPPOc) show less uniform deformation and sharp yielding behavior at low comonomer concentrations [98, 101–103]. The yielding behavior becomes smoother with increasing comonomer content (Fig. 9E–G), and the deformation becomes uniform. The copolymer samples iPPEt, iPPHe, and iPPOc with the highest comonomer concentrations (BE13.1, AH11.2 and DO7.5, respectively) and the iPPBu sample CB12 with 12 mol% butene units show diffuse yielding behavior and uniform deformation.

The values of stress and deformation at yield are reported in Fig. 10. It is apparent that the decrease in stress at yield with increasing comonomer concentration (Fig. 10A, A′) is accomplished with an increase in deformation at yield (Fig. 10B, B′ B″). It is also apparent that each kind of comonomer influences the yield behavior of the copolymers differently. In particular, in the case of highly stereoregular, slightly regiodefective copolymer samples iPPEt, iPPBu, iPPPe, iPPHe, and iPPOc prepared with the catalysts A, C, and D, the decrease in σ_y values is smooth and quasilinear for iPPEt and iPPBu systems and becomes steeper with increasing size of comonomeric units. This decrease is similar for iPPPe and iPPHe samples (Fig. 10A). Moreover, as shown in Fig. 10A′ (inset), in the case of the stereodefective iPP homopolymer sample and iPPEt samples prepared with catalyst B, the decrease in the values of stress at yield as a function of the total concentration of defects is similar to that of regiodefective iPPEt samples prepared with catalyst A.

The values of deformation at yield ε_y for the samples iPPPe, iPPHe, and iPPOc increase with the concentration of pentene, hexene, and octadecene comonomeric units (Fig. 10B), but are nearly constant, or increase only slightly, in the case of iPPEt (Fig. 10B″) and iPPBu (Fig. 10B′) copolymers.

The data in Fig. 10 indicate that the decrease in plastic resistance is generally associated with an increase in deformation at yield. The decrease in plastic resistance, in turn, is related to the level of inclusion in and/or exclusion of comonomeric units from crystals, and to the effective level of disturbance of the defects included in the crystals in the case of inclusion. The almost complete inclusion of butene units in the crystals of the α-form of iPP produces a small decrease in stress at yield (Fig. 10A), and constant values of deformation at yield

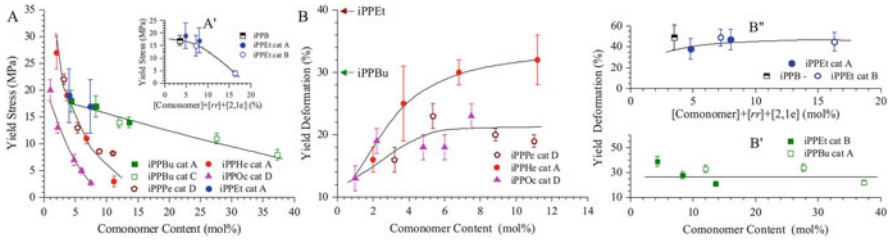

Fig. 10 Values of stress and strain at yield of melt-crystallized films obtained by compression molding of iPP homopolymer iPPB (**A′**, **B″**) and iPPEt (**A**, **A′**, **B**, **B″**), iPPBu (**A**, **B**, **B′**), iPPPe (**A**, **B**), iPPHe (**A**, **B**), and iPPOc (**A**, **B**) copolymer samples prepared with catalysts A–D of Scheme 1. *Arrows* in **B** indicate the average values of deformation at yield of iPPEt (**B″**) and iPPBu (**B′**) samples. Samples iPPA, iPPC, and iPPD are not included because they break before yielding

(Fig. 10B′) that are not dependent on butene concentration. On the other hand, partial (ethylene, pentene, and hexene) or complete (octadecene) exclusion of comonomeric units from the crystals of α- or γ-forms of iPP induces a larger decrease in stress at yield (Fig. 10A), coupled with an increase in yield deformation (Fig. 10B, B″).

As analyzed in the preceding section, melt-crystallized films of these copolymers prepared by compression molding are characterized by different lamellar thicknesses. For semicrystalline polymers, the values of yield stress generally increase with lamellar thickness. In fact, thick lamellae generally entail major crystal stability, and therefore also strong plastic resistance [5–7, 14–19]. The values of yield stress shown in Fig. 10A for the compression-molded samples of copolymers crystallized under similar conditions are reported in Fig. 11 as a function of lamellar thickness, as evaluated from the SAXS profiles shown in Fig. 7. A unique correlation line can be established, regardless of comonomer type. In particular, the logarithm of the yield stress increases as a function of the average values of lamellar thickness according to a sigmoidal master curve. Deviation from this correlation is observed for copolymers of iPPBu with butene concentrations higher than 12–13 mol%, where the lamellar thickness increases and the yield stress decreases with increasing butene concentration. For instance, for samples CB12, CB27.6, and CB37.3 (containing 12, 27.6 and 37.3 mol% of butene, respectively) with high lamellar thickness, the yield stress decreases with increasing lamellar thickness. Exceptions occur at low lamellar thickness for the copolymer iPPPe with pentene content of 11 mol% (sample DP11) and the highly defective copolymers iPPOc with octadecene content of 4.8–6 mol% (samples DO4.8 and DO6.0). These samples show yield stress values that are larger than those expected on the basis of the sigmoidal master curve. However, with further increase in octadecene content (sample DO7.5 with 7.5 mol% comonomer), the value of the yield stress suddenly drops, in apparent agreement with expectation.

These results indicate that, on the one hand, for a homogeneous class of propene-based copolymers (crystallizing in α- and/or γ-forms of iPP under similar conditions) the lamellar thickness controls the level of plastic resistance of the samples.

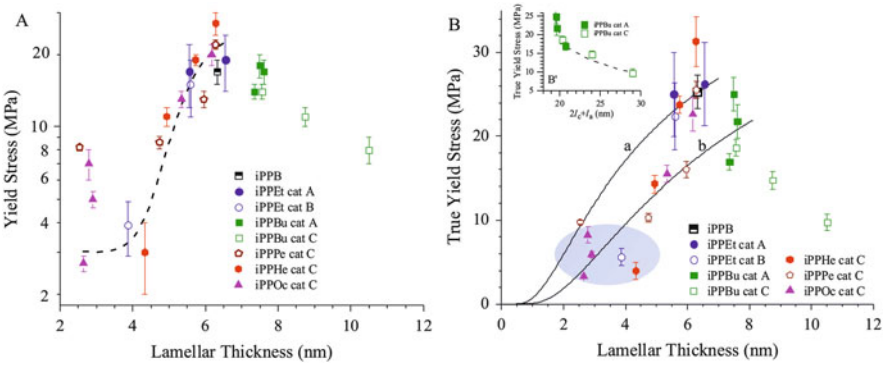

Fig. 11 Values of nominal stress (**A**) and true stress at yield (**B**) of melt-crystallized films obtained by compression molding of iPP homopolymer iPPB and iPPEt, iPPBu, iPPPe, iPPHe, and iPPOc copolymer samples prepared with catalysts A–D of Scheme 1. *Inset* **B′** shows values of true stress at yield of melt-crystallized films obtained by compression molding of iPPBu copolymers as a function of $2l_c + l_a$. *Solid lines* in **B** indicate the theoretical predictions of yield stress on the basis of the crystallographic model [25] based on thermal activation of screw dislocations, according to Eq. 5, by setting the value of the Burgers vector $B = 0.650$ nm, the shear modulus of (040) planes $K = 0.84$ GPa, and the free energy barrier associated with nucleation of [001] dislocations ΔG^* in the range 40–90 kT, namely $\Delta G^* = 59\,kT$ (*curve a*) and $90\,kT$ (*curve b*) [94]. The *shaded area* indicates samples with critical dislocation nuclei (calculated using Eq. 3) too large in size to be acceptable

However, because crystal stability also depends on the concentration and distribution of the structural irregularities, in the case of iPPBu copolymers with a high concentration of butene units, the easy inclusion of comonomers in the unit cell of the α-form of iPP induces formation of lamellar crystals of high thickness but lower plastic resistance (yield stress) than expected for defect-free crystals of homopolymer having identical thickness. This indicates that butene units act as point-like defects in the crystals and, therefore, induce a decrease in plastic resistance. On the other hand, polymorphism and the amorphous phase placed between lamellar crystals could also play a role [5–7, 14–19]. This is evidenced in the case of iPPOc copolymers with 4.8 and 6 mol% of octadecene. For these copolymers, the yield stress is higher than expected on the basis of the low values of lamellar thickness. Because the long branches are rejected from the crystals, their confinement in the amorphous interlamellar layers close to the fold surfaces produces an indirect increase in resistance to plastic deformation of the crystals, probably as a result of topological restraints. Instead, polymorphism is involved for iPPPe and iPPOc copolymer samples DP11 and DO7.5 (with 11 and 7.5 mol% of pentene and octadecene units, respectively). As shown in Fig. 3, the sample DP11 crystallizes in a mixture of crystals of α-form and trigonal form [103, 104] (Fig. 2C), whereas the sample DO7.5 crystallizes in a mixture of α-form and the second mesophase of iPP [102] (Fig. 2D). Both the trigonal form and the mesomorphic form that crystallize along with the α-form are characterized by partial inclusion of comonomers in the crystalline domains. The trigonal form of the iPPPe copolymer is characterized by

long-range order in two dimensions for the positioning of chain axes of the 3/1 helices [162] (Fig. 2C); the new mesomorphic form of the iPPOc sample, instead, presents no lateral order in the position of chain axes, and only an average periodicity parallel to chain axes of 3/1 helices [162] (Fig. 2D). As a consequence, the presence of a second polymorph increases the resistance to plastic deformation in the iPPPe sample partially crystallized in the trigonal form, but decreases the plastic resistance in the iPPOc samples partially crystallized in the new mesophase.

At temperatures higher than the glass transition, the strong dependence of yield stress on lamellar thickness, which is generally observed for semicrystalline polymers and in our copolymers in particular (Fig. 11A), entails a yield behavior possibly controlled by activation of plastic deformation of lamellar crystals through crystallographic slip processes [5–7, 14–19, 25]. Crystallographic slip processes, in turn, are facilitated by nucleation and propagation of dislocations and/or defects [25, 74–76]. According to this mechanism, the stress at yield corresponds to the point of the stress–strain curve at which local stress reaches the level of the critical resolved shear stress for the easiest slip system. This level is, in turn, controlled by nucleation and propagation of dislocations within deforming crystals [5–7, 14–19, 25, 84]. Therefore, the strong dependence of the yield stress of polymer crystals on lamellar thickness (Fig. 11A) can be explained by the fact that the critical stress for activation of chain slip is directly related to the strong dependence of the rate of nucleation of dislocations on the thickness of the crystals.

The minimum stress required for nucleation and activation of a new dislocation at the edges of lamellar crystals and the relationship between this stress to crystal thickness can be predicted using the model of Young [25], successively refined by Shadrake and Guiu [93]. According to this model, any contribution from the chains in the amorphous phase to the yield stress is neglected in a first approximation. The role of amorphous chains is merely as force transmitters, because the modulus of the amorphous phase above T_g is an order of magnitude lower than the modulus of crystalline phase. The model assumes that deformation occurs by $\{hk0\}$ <001> chain direction slip, resulting in the formation of [001] screw dislocations (i.e., dislocations parallel to the chain axes) [25]. The Burgers vector **B**, parallel to the chain axis (Fig. 12A) at distance r from the dislocation, has magnitude B and generally spans only a small integer number n ($n = 1,2$) of chain periodicities c. The nucleation and activation of [001] dislocations of length l_c coincident with the lamellar thickness is a thermally activated process requiring a critical level τ^* of shear stress. Within the model, only the value of τ^* matters because the intrinsic movement of already formed dislocations occur at Peierls–Nabarro stress (i.e., at a stress level much lower than τ^*) (Fig. 11A). According to the crystallographic approach, yielding (i.e., the beginning of plastic deformation) starts when the critical resolved shear stress is reached in any family of planes with low τ^*. This corresponds to slip planes coincident with the lattice planes of maximum packing and to slip directions parallel to the lattice directions of maximum packing [5–7, 14–19, 25].

In the simplest approach, the free energy associated with the nucleation of such dislocations can be written as:

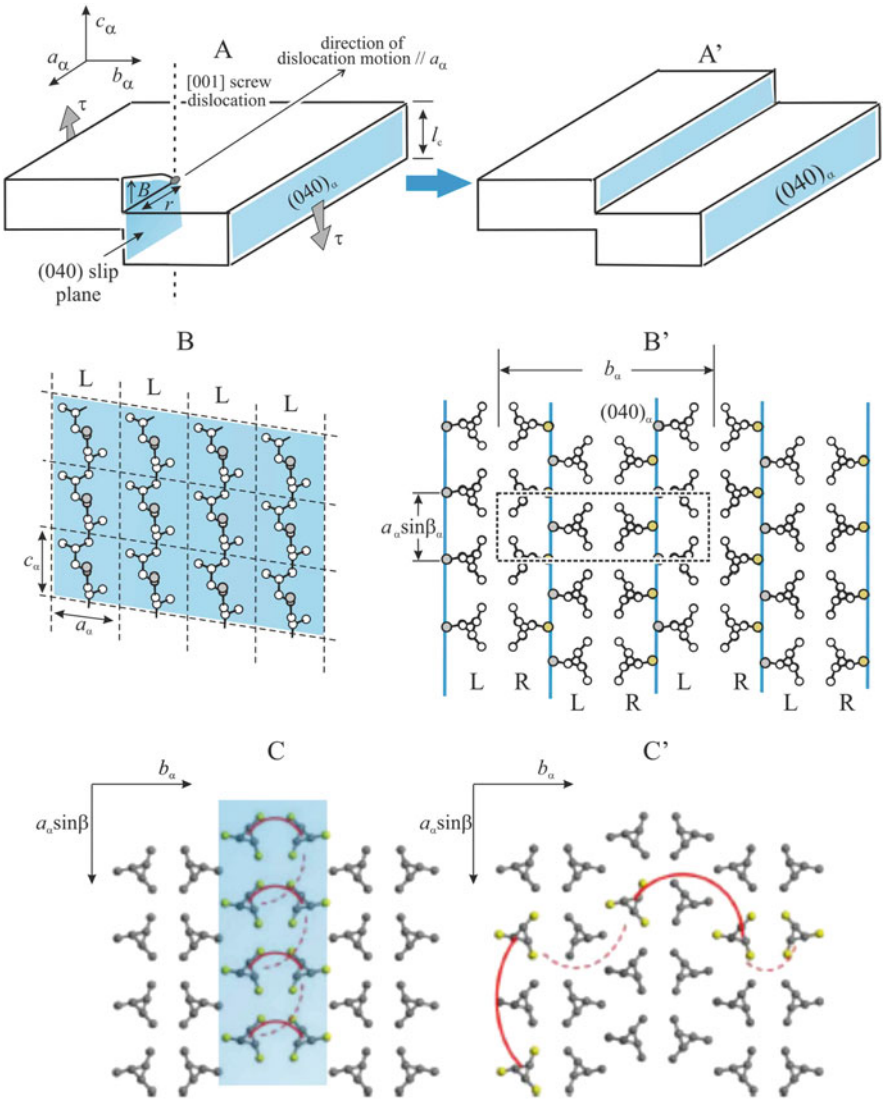

Fig. 12 (**A**) Model of a [001] screw dislocation, nucleated at the edge of a lamellar crystal of iPP in the α-form, that has advanced a distance r inside the crystal parallel to the (040) slip planes, along the slip direction. The length of the dislocation is equal to the crystal thickness l_c, whereas the Burgers vector, parallel to chain axis, has a magnitude equal to the chain periodicity c_α ($B = 0.65$ nm). Lamellar crystals (**A′**) obtained through deformation in the $\{0k0\}<00l>$ chain direction slip leading the dislocation in **A** to emerge at the opposite edge of the crystal and consequent formation of a step. (**B**) The (040) slip planes in two projections parallel (**B**) and perpendicular (**B′**) to the chain axis. Symbols *L* and *R* stand for left- and right-handed helical chains, respectively. Rows $a_\alpha - c_\alpha$ of all left-handed helical chains alternate with rows of chains of opposite chirality forming double layers, delimited by traces of the (040) planes in **B′** [149, 150]. The lattice planes (040) are planes of close packing and the slip direction in **A** is parallel to the lattice direction of maximum packing [149, 150]. (**C**) Schemes of chain folding with adjacent (**C**) and non-adjacent re-entry (**C′**) for the limit-ordered [150, 162] and limit-disordered

$$\Delta G = \frac{KB^2 l_c}{2\pi} \ln \frac{r}{r_0} - l_c B r \tau \tag{2}$$

In Eq. 2, K is the shear modulus associated with the $\{hk0\}<001>$ slip process, r_0 is the core radius of the dislocations (generally assumed to be twice the value of B [26, 94]), and r is the distance of the dislocation from the edge of the crystal (Fig. 12A). The first term corresponds to the elastic strain energy and the second term corresponds to the work performed by the external shear stress. In Eq. 2, the core energy contribution as a result of lattice distortions around the dislocation is neglected. Dislocations are activated when the distance of a dislocation from the edge of the crystal reaches a critical value r^* (size of the critical dislocation nuclei), obtained by setting the derivative of ΔG with respect to r as equal to zero [25]. The obtained value of the critical size of the dislocation r^*, the critical nucleus, is given by:

$$r^* = \frac{KB}{2\pi\tau} \tag{3}$$

By combining Eqs. 2 and 3, the activation barrier of free energy ΔG^* needed to nucleate a dislocation of critical size r^* is obtained as:

$$\Delta G^* = \frac{KB^2 l_c}{2\pi} \left[\ln \left(\frac{r^*}{r_0} \right) - 1 \right] \tag{4}$$

Finally, introducing Eq. 3 into Eq. 4, the value of tensile stress σ_y, which is twice the critical value of the shear stress τ_y (i.e., $\sigma_y = 2\,\tau_y$) according to Tresca's criterion, is obtained as:

$$\sigma_y = \frac{K}{2\pi} \exp \left(- \frac{2\pi \Delta G^*}{l_c K B^2} - 1 \right) \tag{5}$$

Notice that Eq. 5 assumes that the core radius of the dislocation r_0 is equal to twice the length of the Burgers vector B ($2r_0$) [26, 94].

To compare the yield behavior of our samples with the predictions of the crystallographic model based on thermal activation of dislocations (Eq. 5), the values of true stress at yield are needed. In general, the transverse strain of semicrystalline polymers (perpendicular to the stretching direction under uniaxial elongation) decreases with deformation. For rubbery materials at low deformation, the transverse section S of the deformed sample is related to the initial section S_0 of the specimen by the relationship $S = S_0\,(l_0/l)$ where l_0 and l are the initial gauge-

Fig. 12 (continued) [149, 162] α-forms of iPP, respectively. Deformations in the $\{010\}<001>$ chain direction slip comply well with the chain folding scheme with adjacent re-entry **C**. (**C** and **C′** are reproduced from [163], with ACS permissions)

length and the gauge-length in the deformed state, respectively. This relationship entails that the sample is incompressible, that is, that Poisson's ratio is equal to 0.5. However, for semicrystalline polymers, Poisson's ratio changes during deformation from the maximum value of 0.5 to values close to zero, as a result of volume expansion caused by crazing, cracks, and voids [164]. We checked that the deformation of our copolymer samples was largely uniform up to the yield point. Therefore, we corrected the nominal values of stress at yield by the factor l/l_0 to obtain the true stress, implicitly assuming a Poisson's ratio close to 0.5. The obtained values of true stress are reported in Fig. 11B as a function of lamellar thickness.

Representative curves describing the change in yield stress with lamellar thickness according to the crystallographic model based on thermal activation of screw dislocations are also given in Fig. 11B. They were generated using Eq. 5 by fixing the parameters of the model according to the values suggested in the literature for modeling the yield behavior of iPP [94]. For the sake of simplicity and without loss of generality, confining attention to the α-form of iPP, it is assumed that plastic deformation occurs by $\{0k0\}<00l>$ chain direction slip that is parallel to the (040) planes of maximum packing of the iPP α-form, with the [001] screw dislocation parallel to the chain axes (Fig. 12A, B, B′). This deformation mechanism complies well with the chain folding scheme for the α-form of iPP, characterized by adjacent re-entry (Fig. 12C), as proposed by Corradini [165–167] and confirmed by double quantum ^{13}C–^{13}C solid state NMR [163]. In particular, the value of the Burgers vector B is set equal to 0.650 nm, corresponding to the chain periodicity of iPP in the α-form [149, 150]. The values for the energy barrier ΔG^* were selected in the typical range of 40–90 kT [94] associated with the thermal nucleation of dislocation at laboratory time scales, namely $\Delta G^* = 59$ and 90 kT, respectively. The values of shear modulus for the (040) lattice planes was set at 0.84 GPa, in agreement with values suggested in the literature for iPP (in the range 0.84–1.0 GPa) [94].

A screw dislocation scheme similar to that of Fig. 12 for the α-form of iPP can also be proposed for the γ-form [151, 152], considering that the chain axes in the γ-form are directed along the diagonal of the C face of the orthorhombic unit cell (Fig. 2B). This entails that the screw dislocations parallel to the chain axes are parallel to the [110] and/or $\left[\bar{1}10\right]$ lattice directions and that plastic deformation occurs by $\{00l\}<110>$ chain direction slip (i.e., parallel to the (008) planes of the γ-form). A further adjustment of the crystallographic model entails that the chain axes, and therefore the Burgers vector, lie at a tilted angle of ≈40° to the normal of the basal face of the lamellar crystals.

With the exception of iPPBu copolymer samples with high butene content, the results of the model appear to be in good agreement with experimental results in all cases (Fig. 11B). This indicates that, in spite of the simplicity of the model, the crystallographic model describes well (without making any fitting attempt) the yield behavior of our samples, regardless of the kind and concentration of comonomeric units. This result is noteworthy, especially considering that the copolymers are characterized by different degrees of inclusion/exclusion of the

comonomeric units in the crystals. This inclusion generates different concentrations and kinds of structural disorder and, therefore, the crystals are characterized by different intrinsic stabilities. Moreover, the spread of experimental data in Fig. 11B is also the result of measurements being performed in independent experiments, at ambient conditions (room temperature) subject to significant thermal fluctuations (±5°C) and on samples adopting slightly different deformation rates, although the ratio between the deformation rate v_{def} and initial gauge length l_0 was fixed at 10 ($v_{def}/l_0 = 10$). Minor errors also arise from the approximate evaluation of true stress at yield utilizing a Poisson ratio of 0.5 and the approximate evaluation of lamellar thickness l_c, since the volume fraction of the crystalline phase is slightly lower than the crystallinity index x_c resultant from WAXS analysis. In fact, using values of the Poisson ratio close to 0.4, typical for semicrystalline polymers at low deformations, and/or values of lamellar thickness evaluated from the one-dimensional correlation function [120, 121], the dislocation model can equally well describe the yield behavior of our samples, using values close to 0.84 GPa for the shear modulus for the (040) planes K and in the range 59–90 kT for the free energy barrier associated with the nucleation of [001] dislocations ΔG^*.

We also checked that the size of the critical dislocation nucleus r^* calculated using Eq. 2 is in all cases in the range 5–10 nm, that is, less than the typical size of crystal blocks in lamellar crystals (15–30 nm) [100, 101], as estimated from the WAXS profiles using the Scherrer formula (the width at mid-height of the equatorial reflections are all in the range 0.4–0.8°; see Fig. 2). Only in the case of the samples with high comonomer content, having low lamellar thickness and low crystallinity, do the values of r^* exceed 15 nm. These samples are indicated in Fig. 10B and correspond to samples of iPPOc with octene content higher than 4 mol% (samples DO4.8, DO6.0, and DO7.5), iPPEt with ethylene content of 13 mol% (sample BE13.1), and iPPPe and iPPHe with ≈11 mol% comonomer units (samples DP11 and AH11.2, respectively). Because the value of the critical dislocation nuclei r^* cannot be greater than the dimensions of a crystal block, the good agreement of the model with experimental data for low values of lamellar thickness should be considered with caution. In fact, the presence of crystals in a different polymorph, namely the γ-form for sample AH11.2, the trigonal form for samples DP11 and AH11.2 (Fig. 2C), and the new mesophase for sample DO7.5 (Fig. 2D), could completely alter the $\{0k0\}<00l>$ chain direction slip mechanism of [001] dislocation proposed for the α-form (Fig. 12A, B). Furthermore, the rejection of branches outside the crystals, close to the fold surfaces, increases the plastic resistance of the amorphous phase and overcomes the role of crystals in the yield mechanism [14–19]. This indicates that, for samples with low crystallinity in which the lamellar crystals have a thickness lower than the threshold value of 4–5 nm, the role of the amorphous phase in the yield behavior cannot be neglected.

A further exception occurs at high lamellar thickness for the iPPBu samples with butene concentrations higher than 12 mol%. In particular, the decrease in true stress values with increasing lamellar thickness cannot be explained by resorting to the crystallographic model. The yield behavior of these systems derives from the easy

inclusion of butene units in crystals of the α-form. This inclusion, on the one hand, increases lamellar thickness while decreasing the stability of crystals and, on the other hand, increases lattice resistance to the gliding of dislocations because point defects act as Peierls barriers. Therefore, the observed values of yield stress achieved in these samples is the resultant of two competitive effects, the decrease in lamellar stability and the simultaneous increment of barriers to the movement of dislocations, because butene units in the crystals act as localized obstacles. An alternative or complementary mechanism subtending the yield behavior of these samples could involve the deformation modes of the amorphous phase, such as interlamellar separation and interlamellar slip (Fig. 1E, F) [5–7, 14–19]. These modes become active whenever the easiest movement at the mesoscale is stretching of the intralamellar amorphous chains connecting adjacent layers instead of crystal slip. To form an efficient tie, a chain emerging from a lamellar crystal (thickness l_c) should travel across the amorphous layer (thickness l_a) and enter a new crystalline lamella (thickness l_c). The higher the number density of tie chains, the higher the yield stress level. Moreover, the higher the degree of separation of adjacent lamellae, the lower the number density of tie chains. Therefore, the probability of formation of a tie chain is expected to decrease with the quantity $2l_c + l_a$. The decrease in true stress at yield of these samples with increase in $2l_c + l_a$ (shown in Fig. 11B′, inset), is in agreement with the above argument.

It is worth noting that, using the Eyring formalization of thermally activated processes [168, 169], the temperature and strain rate dependence of yield stress of the iPP homopolymer indicate that two basic processes intervene in the stress response of a semicrystalline polymer [26–28, 62–65]. The first process involves intralamellar deformations or crystal slips, the mechanisms of which have been already detailed. The second process involves interlamellar deformations and is somehow linked to the α-relaxation mechanism of iPP [170]. This relaxation involves motion of the 3/1 helical chains in the crystals through the combined effect of 120° rotations around the chain axis and $c/3$ translation parallel to the chain axis [171]. These jumps result in chain diffusion through the crystals and necessarily involve the mobility of repeating units in the constrained amorphous zone surrounding the crystal [171]. In the case of iPP homopolymer, the intralamellar deformation contributes to the yield stress at high temperatures or low strain rates [62–65]. Crystal slip also participates at lower temperatures and/or high strain rates, but the main process contributing to the observed yield stress is the interlamellar process [62–65]. Therefore, in the case of iPP homopolymer, the contribution of α-relaxation and consequent participation of the amorphous phase to the yield stress should not be neglected at deformation temperatures close to ambient.

In the case of copolymers, the α-relaxation mechanism is expected to contribute actively to yield stress only at low comonomer concentration. With increasing concentration of comonomeric units, this mechanism becomes less important, regardless of the degree of inclusion/exclusion of comonomers in/from the crystals. In fact, chain diffusion inside the crystals associated with α-relaxation is prevented by the large steric hindrance caused by comonomers located inside the crystals in

the case of inclusion, and by comonomers located in the amorphous regions close to the fold surfaces in the case of exclusion. The different degrees of participation of the α-relaxation process to the yielding behavior of our copolymers can explain the bifurcation of the experimental values of yield stress shown in Fig. 11B. For lamellar thicknesses higher than 5 nm, samples with lower content of comonomeric units show values of yield stress close to the curve generated by setting the free energy barrier for nucleation of dislocations $\Delta G^* = 59\,kT$ (Fig. 11B, curve a), whereas the samples with higher content of comonomeric units follow the curve generated by setting $\Delta G^* = 90\,kT$ (Fig. 11B, curve b). We argue that the lower free energy barrier associated with the thermal nucleation of dislocations observed for the samples of curve a is a result of participation of the α-relaxation process to their yield behavior. Lack of this participation, for the samples of the curve b, results in an increase in the free energy barrier.

5 Concluding Remarks

The yield behavior in tensile experiments of a wide class of semicrystalline polymers is analyzed in the framework of a crystallographic micromechanical model based on the thermal nucleation of dislocations. The samples are isotactic copolymers of propene with ethylene (iPPEt), 1-butene (iPPBu), 1-pentene (iPPPe), 1-hexene (iPPHe), and 1-octadecene (iPPOc) and possess a random distribution of comonomeric units and tailored concentrations of stereo- and regiodefects.

It has been shown that the decrease in plastic resistance depends on the level of inclusion/exclusion of the comonomeric units in/from the crystals and on the effective level of disturbance of the comonomers included in the crystals. Moreover, a remarkable dependence of yield stress on lamellar thickness has been demonstrated. In particular, we have shown that, in all cases, the values of yield stress decrease with lamellar thickness. By contrast, in the case of iPPBu copolymers, the almost complete inclusion of butene units in the crystals of α-form produces a decrease in stress at yield and simultaneous increase in lamellar thickness.

According to the crystallographic approach, the phenomenon of yielding marks the beginning of plastic flow through occurrence of diffuse crystal slip processes, facilitated by the movement of dislocations, nucleation of new dislocations at the edge of lamellar crystals, and participation of the amorphous component through interlamellar slip or interlamellar rotation. Therefore, the thickness and intrinsic stability of lamellar crystals and the intrinsic mobility of the constrained interlamellar amorphous phase play key roles. Applying these concepts, we have shown that, except for iPPBu copolymers with high butene content, in our copolymers the yield behavior is largely controlled by the activation of plastic deformation of the crystals through crystallographic slip processes, involving, in turn, nucleation of new dislocations. However, for highly defective copolymers of low crystallinity, forming lamellar crystals of low thickness, the role of the deformation

modes of the amorphous phase, such as interlamellar separation and interlamellar slip, should not be neglected. In the case of iPPBu, the beginning of plastic deformation is also controlled by the increase in lattice resistance to glide of dislocations as a result of the butene units in the crystals acting as Peierls barriers.

References

1. Keller A (1968) Polymer crystals. Rep Prog Phys 31:623–704
2. Ward IM, Sweeney J (2004) An introduction to the mechanical properties of solid polymers, 2nd edn. Wiley, Chichester
3. Peterlin A (1977) Plastic deformation of crystalline polymers. Polym Eng Sci 17:183–193
4. Peterlin A (1975) Composite structure of fibrous material. Adv Chem Ser 142:1–13
5. Oleinik EF, Rudnev SN, Salamatina OB (2007) Evolution in concepts concerning the mechanism of plasticity in solid polymers after the 1950s. Polym Sci Ser A 49:1302–1327
6. Haudin JM (1982) Plastic deformation of semi-crystalline polymers. In: Escaig B, G'Sell C (eds) (1982) Plastic deformation of amorphous and semi-crystalline materials. Les Editions de Physique, Paris, pp 291–311
7. Bartczak Z, Galeski A (2010) Plasticity of semicrystalline polymers. Macromol Symp 294:67–90
8. Lin L, Argon AS (1994) Structure and plastic deformation of polyethylene. J Mater Sci 29:294–323
9. Crist B (1993) Plastic deformation in material science and technology. In: Thomas EL (ed) A comprehensive treatment, vol 12. VCH, New York, pp 427–470
10. Lee BJ, Argon AS, Parks DM, Ahzi S, Bartczak Z (1993) Simulation of large strain plastic deformation and texture evolution in high density polyethylene. Polymer 34:3555–3575
11. Lee BJ, Argon AS, Ahzi S (1993) Micromechanical modeling of large plastic deformation and texture evolution in semi-crystalline polymers. J Mech Phys Solids 41:1651–1687
12. Hay IL, Keller A (1965) Polymer deformation in terms of spherulites. Kolloid-Zu Z Polymere 204:43–74
13. Breese DR, Beaucage G (2004) Curr Opinion Solid State Mater Sci 8:439–448
14. Séguéla R (2007) Plasticity of semi-crystalline polymers: crystal slip versus melting-recrystallization. e-Polymers 032:1–20
15. Seguela R (2002) Dislocation approach to the plastic deformation of semicrystalline polymers: kinetic aspects for polyethylene and polypropylene. J Polym Sci B Polym Phys 40:593–601
16. Séguéla R (2005) Critical review of the molecular topology of semicrystalline polymers: the origin and assessment of intercrystalline tie molecules and chain entanglements. J Polym Sci B Polym Phys 43:1729–1748
17. Liu B, Zhang L, Gao H (2006) Poisson ratio can play a crucial role in mechanical properties of biocomposites. Mech Mater 38:1128–1142
18. Liu B, Feng X, Zhang S-M (2009) The effective Young's modulus of composites beyond the Voigt estimation due to the Poisson effect. Compos Sci Tech 69:2198–2204
19. Gorbatikh L, Pingle P (2007) On incompressibility of a matrix in naturally occurring composites. Appl Phys Lett 91:241913
20. Peterlin A (ed) (1971) Plastic deformation of polymers. Marcel Dekker, New York
21. Peterlin A (1987) In: Mark HF, Bikales NM, Overberger CG, Menges G, Kroschwitz JI (eds) Encyclopedia of polymer science and engineering. Wiley, New York, pp 72–94
22. Samuels RJ (1974) Structured polymer properties. Wiley, New York
23. Bueche F (1956) Young's modulus of semicrystalline polymers. J Polym Sci A Polym Chem 22:113–122

24. Halpin JC, Kardos JL (1972) Moduli of crystalline polymers employing composite theory. J Appl Phys 43:2235–2241
25. Bowden PB, Young RJ (1974) Deformation mechanisms in crystalline polymers. J Mater Sci 9:2034–2051
26. Schrauwen BAG, Bernard AG, Janssen RPM, Govaert LE, Meijer HEH (2004) Intrinsic deformation behavior of semicrystalline polymers. Macromolecules 37:6069–6078
27. Govaert LE, Meijer HEH (2005) Mechanical performance of polymer systems: the relation between structure and properties. Prog Polym Sci 30:915–938
28. Caelers HJM, Govaert LE, Peters GWM (2016) The prediction of mechanical performance of isotactic polypropylene on the basis of processing conditions. Polymer 83:116–128
29. Flory PJ, Yoon DY (1978) Molecular morphology in semicrystalline polymers. Nature 272:226–229
30. Gent AN, Madan S (1989) Plastic yielding of partially crystalline polymers. J Polym Sci B Polym Phys 27:1529–1542
31. Young RJ (1974) A dislocation model for yield in polyethylene. Philos Mag 30:85–94
32. Galeski A, Bartczak Z, Argon AS, Cohen RE (1992) Deformation mechanisms and plastic resistance in single-crystal-textured high-density polyethylene. Macromolecules 25:5705–5718
33. Hiss R, Hobeika S, Lynn C, Strobl G (1999) Network stretching, slip processes, and fragmentation of crystallites during uniaxial drawing of polyethylene and related copolymers. A comparative study. Macromolecules 32:4390–4403
34. Men Y, Strobl GJ (2001) Critical strains determining the yield behavior of s-PP. J Macromol Sci Phys B40:775–796
35. Hughes DJ, Mahendrasingam A, Oatway WB, Heeley EL, Martin C, Fuller W (1997) A simultaneous SAXS/WAXS and stress-strain study of polyethylene deformation at high strain rates. Polymer 38:6427–6430
36. Yamada M, Miyasaka K, Ishikawa K (1971) Redrawing of oriented polyethylene film. J Polym Sci B Polym Phys 9:1083–1096
37. Takahashi Y, Ishida T (1988) J Polym Sci B Polym Phys 26:2267–2277
38. Stoclet G, Seguela R, Lefebvre JM, Elkoun S, Vanmansart C (2010) Strain-induced molecular ordering in polylactide upon uniaxial stretching. Macromolecules 43:1488–1498
39. Seguela R (2005) On the strain-induced crystalline phase changes in semi-crystalline polymers: mechanisms and incidence on the mechanical properties. J Macromol Sci C Polym Rev J 45:263–287
40. De Rosa C, Auriemma F (2007) Stress-induced phase transitions in metallocene-made isotactic polypropylene. Lect Notes Phys 714:345–371
41. De Rosa C, Auriemma F (2006) Structural–mechanical phase diagram of isotactic polypropylene. J Am Chem Soc 128:11024–11025
42. De Rosa C, Auriemma F, de Ballesteros OR (2006) A microscopic insight into the deformation behavior of semicrystalline polymers: the role of phase transitions. Phys Rev Lett 96:167801–167804
43. De Rosa C, Auriemma F (2012) The deformability of polymers: the role of disordered mesomorphic crystals and stress-induced phase transformations. Angew Chem Int Ed 124:1233–1237
44. Liu Y, Kennard CHL, Truss RW, Carlos NJ (1997) Characterization of stress-whitening of tensile yielded isotactic polypropylene. Polymer 38:2797–2805
45. Hay IL, Keller A (1970) Mechanically induced twinning and phase transformations. J Polym Sci C Polym Symp 30:289–295
46. Frank FC, Keller A, O'Connor A (1958) Deformation processes in polyethylene interpreted in terms of crystal plasticity. Philos Mag 3:64–74
47. Kiho H, Peterlin A, Geil PH (1964) Polymer deformation. VI. Twinning and phase transformation of polyethylene single crystals as a function of stretching direction. J Appl Phys 35:1599–1605

48. Allan P, Crellin EB, Bevis M (1973) Stress-induced twinning and phase transformations in polyethylene single crystals. Philos Mag 27:127–145
49. Butler MF, Donald AM, Bras W, Mant GR, Derbyshire GE, Ryan AJ (1995) A real-time simultaneous small- and wide-angle X-ray scattering study of in-situ deformation of isotropic polyethylene. Macromolecules 28:6383–6393
50. Butler MF, Donald AM, Ryan AJ (1997) Time resolved simultaneous small- and wide-angle X-ray scattering during polyethylene deformation: 1. Cold drawing of ethylene-α-olefin copolymers. Polymer 38:5521–5538
51. Butler MF, Donald AM (1998) A real-time simultaneous small- and wide-angle X-ray scattering study of in situ polyethylene deformation at elevated temperatures. Macromolecules 31:6234–6249
52. Butler MF, Donald AM, Ryan AJ (1998) Time resolved simultaneous small- and wide-angle X-ray scattering during polyethylene deformation -- II. Cold drawing of linear polyethylene. Polymer 39:39–52
53. Ran S, Zong X, Fang D, Hsiao BS, Chu B, Phillips RA (2001) Structural and morphological studies of isotactic polypropylene fibers during heat/draw deformation by in-situ synchrotron SAXS/WAXD. Macromolecules 34:2569–2578
54. Ciferri A (1963) The α↔ transformation in keratin. Trans Faraday Soc 59:562–569
55. Ciferri A, Smith KJ Jr (1964) Phase changes in fibrous macromolecular systems and associated elasticity. Model phase diagrams. J Polym Sci A 2:731–753
56. Tashiro K, Nakai Y, Kobayashi M, Tadokoro H (1980) Solid-state transition of poly(butylene terephthalate) induced by mechanical deformation. Macromolecules 13:137–145
57. Auriemma F, De Rosa C (2003) New concepts in thermoplastic elastomers: the case of syndiotactic polypropylene, an unconventional elastomer with high crystallinity and large modulus. J Am Chem Soc 125:13143–13147
58. Auriemma F, De Rosa C (2003) Time-resolved study of the martensitic phase transition in syndiotactic polypropylene. Macromolecules 36:9396–9410
59. Auriemma F, De Rosa C, Esposito S, Mitchell GR (2007) Polymorphic superelasticity in semicrystalline polymers. Angew Chem Int Ed 46:4325–4328
60. Kazmierczak T, Galeski A, Galeski A, Argon AS (2005) Plastic deformation of polyethylene crystals as a function of crystal thickness and compression rate. Polymer 46:8926–8936
61. Argon AS, Galeski A, Kazmierczak T (2005) Rate mechanisms of plasticity in semicrystalline polyethylene. Polymer 46:11798–11805
62. Schrauwen BAG, van Breemen LCA, Spoelstra AB, Govaert LE, Peters GWM, Meijer HEH (2004) Structure, deformation, and failure of flow-oriented semicrystalline polymers. Macromolecules 37:8618–8633
63. Sedighiamiri A, Govaert LE, Kanters MJW, van Dommelen JAW (2012) Micromechanics of semicrystalline polymers: yield kinetics and long-term failure. J Polym Sci B Polym Phys 50:1664–1679
64. van Erp TB, Cavallo D, Peters GWM, Govaert LE (2012) Rate-, temperature-, and structure-dependent yield kinetics of isotactic polypropylene. J Polym Sci B Polym Phys 50:1438–1451
65. van Breemen LCA, Engels TAP, Klompen ETJ, Senden DJA, Govaert LE (2012) Rate- and temperature-dependent strain softening in solid polymers. J Polym Sci B Polym Phys 50:1757–1771
66. Hobeika S, Men Y, Strobl G (2000) Temperature and strain rate independence of critical strains in polyethylene and poly(ethylene-*co*-vinyl acetate). Macromolecules 33:1827–1833
67. Brooks NWJ, Mukhtar M (2000) Temperature and stem length dependence of the yield stress of polyethylene. Polymer 41:1475–1480
68. Peterson JM (1966) Thermal initiation of screw dislocations in polymer crystal platelets. J Appl Phys 37:4047–4050
69. Peterson JM (1968) Peierls stress for screw dislocations in polyethylene. J Appl Phys 39:4920–4928

70. Crist B, Fisher CJ, Howard P (1989) Mechanical properties of model polyethylenes: tensile elastic modulus and yield stress. Macromolecules 22:1709–1718
71. Darras O, Seguela R (1993) Tensile yield of polyethylene in relation to crystal thickness. J Polym Sci B Polym Phys 31:759–766
72. O'Kane WJ, Young RJ, Ryan AJ (1995) The effect of annealing on the structure and properties of isotactic polypropylene films. J Macromol Sci Phys 34:427–458
73. Bartczak Z, Argon AS, Cohen RE (1992) Deformation mechanisms and plastic resistance in single-crystal-textured high-density polyethylene. Macromolecules 25:5036–5053
74. Gleiter H, Argon AS (1971) Plastic deformation of polyethylene crystals. Philos Mag 24:71–80
75. Lewis D, Wheeler EJ, Maddams WF, Preedy JE (1972) Comparison of twinning produced by rolling and annealing in high- and low-density polyethylene. J Polym Sci A-2 Polym Phys 10:369–373
76. Young RJ, Bowden PB, Ritchie J, Rider RJ (1973) Deformation mechanisms in oriented high-density polyethylene. J Mater Sci 8:23–36
77. Gaucher-Miri V, Seguela R (1997) Tensile yield of polyethylene and related copolymers: mechanical and structural evidences of two thermally activated processes. Macromolecules 30:1158–1167
78. Seguela R, Gaucher-Miri V, Elkoun S (1998) Plastic deformation of polyethylene and ethylene copolymers. Part I. Homogeneous crystal slip and molecular mobility. J Mater Sci 33:1273–1279
79. Seguela R, Elkoun S, Gaucher-Miri V (1998) Plastic deformation of polyethylene and ethylene copolymers. Part II. Heterogeneous crystal slip and strain-induced phase change. J Mater Sci 33:1801–1807
80. Peterlin A (1971) Molecular model of drawing polyethylene and polypropylene. J Mater Sci 6:490–508
81. Peterlin A (1965) Crystalline character in polymers. J Polym Sci Part C Polym Symp 9:61–89
82. Bartczak Z, Cohen RE, Argon AS (1992) Evolution of the crystalline texture of high-density polyethylene during uniaxial compression. Macromolecules 25:4692–4704
83. Bartczak Z, Lezak E (2005) Evolution of lamellar orientation and crystalline texture of various polyethylenes and ethylene-based copolymers in plane-strain compression. Polymer 46:6050–6063
84. Galeski A (2003) Strength and toughness of crystalline polymer systems. Prog Polym Sci 28:1643–1699
85. Men Y, Rieger J, Strobl G (2003) Role of the entangled amorphous network in tensile deformation of semicrystalline polymers. Phys Lett 91:95502
86. Al-Hussein M, Strobl G (2002) Strain-controlled tensile deformation behavior of isotactic poly(1-butene) and its ethylene copolymers. Macromolecules 35:8515–8520
87. Men Y, Strobl G (2003) Critical strains in poly(ε-caprolactone) and blends with poly(vinyl methyl ether) and poly(styrene-co-acrylonitrile). Macromolecules 36:1889–1898
88. Hong K, Rastogi A, Strobl G (2004) A model treating tensile deformation of semicrystalline polymers: quasi-static stress–strain relationship and viscous stress determined for a sample of polyethylene. Macromolecules 37:10165–10174
89. Brown N, Ward IM (1983) The influence of morphology and molecular weight on ductile-brittle transitions in linear polyethylene. J Mater Sci 18:1405–1420
90. Seguela R, Darras O (1994) Phenomenological aspects of the double yield of polyethylene and related copolymers under tensile loading. J Mater Sci 29:5342–5347
91. Bartczak Z (2005) Influence of molecular parameters on high-strain deformation of polyethylene in the plane-strain compression. Part II. Strain recovery. Polymer 46:10339–10354
92. Bowden B, Young RJ (1971) Critical resolved shear stress for [001] slip in polyethylene. Nature 229:23–25
93. Shadrake LG, Guiu F (1976) Dislocations in polyethylene crystals: line energies and deformation modes. Philos Mag 34:565–581

94. O'Kane WJ, Young RJ (1995) The role of dislocations in the yield of polypropylene. J Mater Sci Lett 14:433–435
95. Sirotkin RO, Brooks NW (2001) The effects of morphology on the yield behaviour of polyethylene copolymers. Polymer 42:3791–3797
96. Popli R, Mandelkern L (1987) Influence of structural and morphological factors on the mechanical properties of the polyethylenes. J Polym Sci B Polym Phys 25:441–483
97. De Rosa C, Auriemma F, de Ballesteros OR, Resconi L, Camurati I (2007) Crystallization behavior of isotactic propylene-ethylene and propylene-butene copolymers: effect of comonomers versus stereodefects on crystallization properties of isotactic polypropylene. Macromolecules 40:6600–6616
98. De Rosa C, Auriemma F, de Ballesteros OR, Resconi L, Camurati I (2007) Tailoring the physical properties of isotactic polypropylene through incorporation of comonomers and the precise control of stereo and regioregularity by metallocene catalysts. Chem Mater 19:5122–5130
99. De Rosa C, Auriemma F, Vollaro P, Resconi L, Guidotti S, Camurati I (2011) Crystallization behavior of propylene-butene copolymers: the trigonal form of isotactic polypropylene and form I of isotactic poly(1-butene). Macromolecules 44:540–549
100. De Rosa C, Auriemma F, Ruiz de Ballesteros O, De Luca D, Resconi L (2008) The double role of comonomers on the crystallization behavior of isotactic polypropylene: propylene-hexene copolymers. Macromolecules 41:2172–2177
101. De Rosa C, Auriemma F, Ruiz de Ballesteros O, Dello Iacono S, De Luca D, Resconi L (2009) Stress-induced polymorphic transformations and mechanical properties of isotactic propylene-hexene copolymers. Cryst Growth Des 9:165–176
102. De Rosa C, Auriemma F, Di Girolamo R, Romano L, De Luca MR (2010) A new mesophase of isotactic polypropylene in copolymers of propylene with long branched comonomers. Macromolecules 43:8559–8569
103. De Rosa C, Auriemma F, Ruiz de Ballesteros O, Di Caprio MR (2012) Crystal structure of the trigonal form of isotactic propylene–pentene copolymers: an example of the principle of entropy–density driven phase formation in polymers. Macromolecules 45:2749–2763
104. De Rosa C, Auriemma F, Talarico G, de Ballesteros OR (2007) Structure of isotactic propylene-pentene copolymers. Macromolecules 40:88531–88532
105. De Rosa C, Auriemma F, Corradini P, Tarallo O, Dello Iacono S, Ciaccia E, Resconi L (2006) J Am Chem Soc 128:80–81
106. De Rosa C, Dello Iacono S, Auriemma F, Ciaccia E, Resconi L (2006) Macromolecules 39:6098–6109
107. Bingel C, Goeres M, Fraaije V, Winter A (1998) Preparation of preparing substituted indanones. International patent application WO 1998/040331
108. Resconi L, Ciaccia E, Fait A (2004) Process for preparing porous polymers and polymers thereof. International patent application WO 2004/092230
109. Resconi L, Guidotti S, Camurati I, Frabetti R, Focante F, Nifant'ev IE, Laishevtsev IP (2005) C1-symmetric heterocyclic zirconocenes as catalysts for propylene polymerization. 2. ansa-zirconocenes with linked diethienocyclopentadienyl-substituted indenyl ligands. Macromol Chem Phys 206:1405–1438
110. Spaleck W, Kueber F, Winter A, Rohrmann J, Bachmann B, Antberg M, Dolle V, Paulus EF (1994) The influence of aromatic substituents on the polymerization behavior of bridged zirconocene catalysts. Organometallics 13:954–963
111. Hosier IL, Alamo RG, Esteso P, Isasi JR, Mandelkern L (2003) Formation of the α and γ polymorphs in random metallocene–propylene copolymers. Effect of concentration and type of comonomer. Macromolecules 36:623–5636
112. Ruiz-Orta C, Alamo RG (2012) Morphological and kinetic partitioning of comonomer in random propylene 1-butene copolymers. Polymer 53:810–822
113. Ruiz-Orta C, Fernandez-Blazquez JP, Pereira EJ, Alamo RG (2011) Time-resolved FTIR spectroscopic study of the evolution of helical structure during isothermal crystallization of

propylene 1-hexene copolymers. Identification of regularity bands associated with the trigonal polymorph. Polymer 52:2856–2868
114. Jeon K, Palza H, Quijada R, Alamo RG (2009) Effect of comonomer type on the crystallization kinetics and crystalline structure of random isotactic propylene 1-alkene copolymers. Polymer 50:832–844
115. Alamo RG, Ghosal A, Chatterjee J, Thompson KL (2005) Linear growth rates of random propylene ethylene copolymers. The changeover from γ dominated growth to mixed (α + γ) polymorphic growth. Polymer 46:8774–8789
116. Alamo RG, VanderHart DL, Nyden MR, Mandelkern L (2000) Morphological partitioning of ethylene defects in random propylene-ethylene copolymers. Macromolecules 33:6094–6105
117. Alamo RG, Mandelkern L (1991) Crystallization kinetics of random ethylene copolymers. Macromolecules 24:6480–6493
118. Covezzi M, Fait A (2001) Process and apparatus for making supported catalyst systems for olefin polymerisation. International patent application WO 01/44319
119. De Rosa C, Auriemma F, Di Capua A, Resconi L, Guidotti S, Camurati I, Nifant'ev IE, Laishevtsev IP (2004) Structure–property correlations in polypropylene from metallocene catalysts: stereodefective, regioregular isotactic polypropylene. J Am Chem Soc 2004 (126):17040
120. Roe R-J (2000) Methods of X-ray and neutron scattering in polymer science. Oxford University Press, New York
121. Stribeck N (2007) X-ray scattering of soft-matter. Springer, Heidelberg
122. Resconi L, Cavallo L, Fait A, Piemontesi F (2000) Selectivity in propene polymerization with metallocene catalysts. Chem Rev 100:1253–1346
123. Fischer D, Mulhaupt R (1994) The influence of regio- and stereoirregularities on the crystallization behaviour of isotactic poly(propylene)s prepared with homogeneous group IVa metallocene/methylaluminoxane Ziegler-Natta catalysts. Macromol Chem Phys 195:1433–1441
124. Thomann R, Wang C, Kressler J, Mulhaupt R (1996) On the γ-phase of isotactic polypropylene. Macromolecules 29:8425–8434
125. Alamo RG, Kim MH, Galante MJ, Isasi JR, Mandelkern L (1999) Structural and kinetic factors governing the formation of the γ polymorph of isotactic polypropylene. Macromolecules 32:4050–4064
126. Auriemma F, De Rosa C (2002) Crystallization of metallocene-made isotactic polypropylene: disordered modifications intermediate between the α and γ forms. Macromolecules 35:9057
127. De Rosa C, Auriemma F, De Lucia G, Resconi L (2005) From stiff plastic to elastic polypropylene: polymorphic transformations during plastic deformation of metallocene-made isotactic polypropylene. Polymer 46:9461–9475
128. De Rosa C, Auriemma F, Paolillo M, Resconi L, Camurati I (2005) Crystallization behavior and mechanical properties of regiodefective, highly stereoregular isotactic polypropylene: effect of regiodefects versus stereodefects and influence of the molecular mass. Macromolecules 38:9143–9154
129. VanderHart DL, Alamo RG, Nyden MR, Kim MH, Mandelkern L (2000) Observation of resonances associated with stereo and regio defects in the crystalline regions of isotactic polypropylene: toward a determination of morphological partitioning. Macromolecules 33:6078–6093
130. Thomann R, Semke H, Maier RD, Thomann Y, Scherble J, Mulhaupt R, Kressler J (2001) Influence of stereoirregularities on the formation of the γ-phase in isotactic polypropene. Polymer 42:4597–4603
131. Nyden MR, Vanderhart DL, Alamo RG (2001) The conformational structures of defect-containing chains in the crystalline regions of isotactic polypropylene. Comput Theor Polym Sci 11:175–189

132. Poon B, Rogunova M, Hiltner A, Baer E, Chum SP, Galeski A, Piorkowska E (2005) Structure and properties of homogeneous copolymers of propylene and 1-hexene. Macromolecules 38:1232–1243
133. Lotz B, Ruan J, Thierry A, Alfonso GC, Hiltner A, Baer E, Piorkowska E, Galeski A (2006) A structure of copolymers of propene and hexene isomorphous to isotactic poly(1-butene) form I. Macromolecules 39:5777–5781
134. Stagnaro P, Boragno L, Canetti M, Forlini F, Azzurri F, Alfonso GC (2009) Crystallization and morphology of the trigonal form in random propene/1-pentene copolymers. Polymer 50:5242–5249
135. Stagnaro P, Costa G, Trefiletti V, Canetti M, Forlini F, Alfonso GC (2006) Thermal behavior, structure and morphology of propene/higher 1-olefin copolymers. Macromol Chem Phys 207:2128–2141
136. Garcia-Penas A, Gomez-Elvira JM, Lorenzo V, Perez E, Cerrada ML (2015) Synthesis, molecular characterization, evaluation of polymorphic behavior and indentation response in isotactic poly(propylene-co-1-heptene) copolymers. Eur Polym J 64:52–61
137. Polo-Corpa MJ, Benavente R, Velilla T, Quijada R, Perez E, Cerrada ML (2010) Development of the mesomorphic phase in isotactic propene/higher alpha-olefin copolymers at intermediate comonomer content and its effect on properties. Eur Polym J 46:1345–1354
138. Palza H, Lopez-Majada JM, Quijada R, Perena JM, Benavente R, Perez E, Cerrada ML (2008) Comonomer length influence on the structure and mechanical response of metallocenic polypropylenic materials. Macromol Chem Phys 209:2259–2267
139. Lopez-Majada JM, Palza H, Guevara JL, Quijada R, Martinez MC, Benavente R, Perena JM, Perez E, Cerrada ML (2006) Metallocene copolymers of propene and 1-hexene: the influence of the comonomer content and thermal history on the structure and mechanical properties. J Polym Sci B Polym Phys 44:1253–1267
140. Garcia-Penas A, Cerrada ML, Gomez-Elvira JM, Perez E (2016) Microstructure and thermal stability in metallocene iPP-materials: 1-pentene and 1-hexene copolymers. Polym Degrad Stab 124:77–86
141. Natta G, Peraldo M, Corradini P (1959) Modificazione mesomorfa smettica del polipropilene isotattico. Rend Accad Naz Lincei 26:14–17
142. Mileva D, Androsch R, Cavallo D, Alfonso GC (2012) Structure formation of random isotactic copolymers of propylene and 1-hexene or 1-octene at rapid cooling. Eur Polym J 48:1082–1092
143. Mileva D, Androsch R (2012) Effect of co-unit type in random propylene copolymers on the kinetics of mesophase formation and crystallization. Colloid Polym Sci 290:465–471
144. Mileva D, Androsch R, Zhuravlev E, Schick C, Wunderlich B (2011) Formation and reorganization of the mesophase of random copolymers of propylene and 1-butene. Polymer 52:1107–1115
145. Mileva D, Cavallo D, Gardella L, Alfonso GC, Portale G, Balzano L, Androsch R (2011) In situ X-Ray analysis of mesophase formation in random copolymers of propylene and 1-butene. Polym Bull 67:497–510
146. Mileva D, Zia Q, Androsch R (2010) Tensile properties of random copolymers of propylene with ethylene and 1-butene: effect of crystallinity and crystal habit. Polym Bull 65:623–634
147. Mileva D, Androsch R, Zhuravlev E, Schick C (2009) Critical rate of cooling for suppression of crystallization in random copolymers of propylene with ethylene and 1-butene. Thermochim Acta 492:67–72
148. Mileva D, Androsch R, Radusch H-J (2008) Effect of cooling rate on melt-crystallization of random propylene-ethylene and propylene-1-butene copolymers. Polym Bull 61:643–654
149. Natta G, Corradini P (1960) Structures and properties of isotactic polypropylene. Nuovo Cimento Suppl 15:40–51
150. Hikosaka M, Seto T (1973) The order of the molecular chains in isotactic polypropylene crystals. Polym J 5:111–127

151. Bruckner S, Meille SV (1989) Non-parallel chains in crystalline γ-isotactic polypropylene. Nature (London) 340:455–457
152. Meille SV, Bruckner S, Porzio W (1990) γ-Isotactic polypropylene. A structure with nonparallel chain axes. Macromolecules 23:4114–4121
153. Balta-Calleja FJ, Vonk CG (1989) X ray scattering of synthetic polymers. Elsevier, Amsterdam
154. Wunderlich B (1980) Macromolecular physics, vol 3. Academic, New York
155. Crist B (2003) Thermodynamics of statistical copolymer melting. Polymer 44:4563–4572
156. Crist B, Claudio ES (1999) Isothermal crystallization of random ethylene–butene copolymers: bimodal kinetics. Macromolecules 32:8945–8951
157. Crist B, Williams DN (2000) Crystallization and melting of model ethylene-butene random copolymers: thermal studies. J Macromol Sci Phys B39:1–13
158. Crist B, Howard PR (1999) Crystallization and melting of model ethylene–butene copolymers. Macromolecules 32:3057–3067
159. Flory PJ (1951) Theory of crystallization in copolymers. Trans Faraday Soc 55:848–857
160. Sanchez IC, Eby RK (1973) Crystallization of random copolymers. J Res Natl Bur St A Phys Chem 77:353–358
161. Sanchez IC, Eby RK (1975) Thermodynamics and crystallization of random copolymers. Macromolecules 8:638–641
162. De Rosa C, Auriemma F (2013) Crystals and crystallinity in polymers: diffraction analysis of ordered and disordered crystals. Wiley, New York
163. Zhen L, You-lee H, Shichen Y, Jia K, Akihiro K, Akihiro O, Toshikazu M (2015) Determination of chain-folding structure of isotactic polypropylene in melt-grown α crystals by ^{13}C–^{13}C double quantum NMR and selective isotopic labeling. Macromolecules 48:5752–5760
164. Nitta KH, Yamana M (2012) Poisson's ratio and mechanical nonlinearity under tensile deformation in crystalline polymers, rheology. In: De Vicente J (ed) Rheology. InTech, Rijeka, Croatia, pp 113–132. Available from: http://www.intechopen.com/books/rheology/poisson-s-ratio-and-mechanical-nonlinearity-undertensile-deformation
165. Petraccone V, Pirozzi B, Meille SV (1986) Analysis of chain folding in crystalline isotactic polypropylene. The implications of tacticity and crystallographic symmetry. Polymer 27:1665–1668
166. Corradini P, Giunchi G, Petraccone V, Pirozzi B, Vidal HM (1980) Structural variations in crystalline isotactic polypropylene (α form) as a function of thermal treatments. Gazz Chim Ital 110:413–418
167. Auriemma F, de Ballesteros OR, De Rosa C, Corradini P (2000) Structural disorder in the α form of isotactic polypropylene. Macromolecules 33:8764–8774
168. Ree T, Eyring H (1955) Theory of non-Newtonian flow. I. Solid plastic system. J Appl Phys 26:793–800
169. Ree T, Eyring H (1955) Theory of non-Newtonian flow. I. Solution system of high polymers. J Appl Phys 26:800–809
170. Séguéla R, Staniek E, Escaig B, Fillon B (1999) Plastic deformation of polypropylene in relation to crystalline structure. J Appl Polym Sci 71:1873–1885
171. Schaefer D, Spiess HW, Suter UW, Fleming WW (1990) Two-dimensional solid-state NMR studies of ultraslow chain motion: glass transition in atactic poly(propylene) versus helical jumps in isotactic poly(propylene). Macromolecules 23:3431–3439